universität wien

MASTERARBEIT / MASTER'S THESIS

Titel der Masterarbeit / Title of the Master's Thesis

„Evaluation of phosphopeptide enrichment strategies for perturbation studies on *in vitro* systems employing ion mobility mass spectrometry "

verfasst von / submitted by

Patricia Bortel BSc

angestrebter akademischer Grad / in partial fulfilment of the requirements for the degree of

Master of Science (MSc)

Wien, 2020

Studienkennzahl lt. Studienblatt / degree programme code as it appears on the student record sheet:	A 066 862
Studienrichtung lt. Studienblatt / degree programme as it appears on the student record sheet:	Chemie
Betreut von / Supervisor:	Univ.-Prof. Dr. Christopher Gerner

Table of contents

Abstract

Protein phosphorylation, being the most widespread posttranslational protein modification, is a key process in cellular signaling. Influencing cell metabolism, proliferation and apoptosis, its regulation is a sophisticated cascade process and the disruption of its regulatory pathways is associated with various diseases. The identification of regulatory protein phosphorylation sites is crucial for understanding cellular signaling. Phosphoproteomic workflows including analysis by mass spectrometry facilitate the identification of phosphorylated proteins and peptides. As phosphopeptides are present in a sub-stoichiometric manner, specific phosphopeptide enrichment strategies are employed, increasing sensitivity towards phosphopeptide species. In order to optimize a phosphoproteomic workflow in terms of enrichment specificity, robustness and proteolytic digestion efficiency, different proteolytic digestion conditions in combination with subsequent titanium dioxide affinity chromatography based phosphopeptide enrichment were evaluated. The evaluation was performed using an *in vitro* Jurkat cell line model, performing a perturbation study with a phorbol ester as a chemical trigger in order to gain insights into the biological mechanisms driving differentiation of T-lymphocytes. For the evaluation of the drawbacks of normal proteomic analyses for the identification of phosphorylated peptides, results from the obtained phosphoproteome were compared against a background proteome. Sample analysis was performed employing "state-of-the-art" ion mobility mass spectrometry. Additionally, fluorescence cell imaging was performed. Out of the evaluated phosphoproteomic workflows, the overnight digest in combination with titanium dioxide phosphopeptide enrichment yielded the most peptide identifications. A phosphopeptide enrichment factor of 98%, with a total of 11,110 phosphopeptides with 70% class I phosphopeptides, exhibiting highly confident phosphosite positions, was obtained. While the regular proteome showed, as expected, only minor alterations due to the short phorbol ester treatment of three hours, which is not sufficient for greatly altering protein expression, phosphopeptide regulations including phorbol ester binding and endomembrane proteins confirmed a successful treatment, strongly supported by the obtained fluorescence cell images which showed major disturbances in the endomembrane system. Annotation of the identified phosphosites was evaluated via PhosphoSitePlus, highlighting the need for functional phosphoproteomic analyses as half of the phosphosites were not annotated with a function or not annotated at all. The optimized phosphoproteomic workflow was demonstrated to be an important tool for the investigation and comprehensive interpretation of cellular signaling events in proteomic studies.

Zusammenfassung

Die Phosphorylierung von Proteinen ist eine der häufigsten posttranslationalen Modifikationen und stellt einen Schlüsselprozess in der zellulären Signalweiterleitung dar. Sie beeinflusst Prozesse wie Zellmetabolismus, -proliferation und Apoptose und eine Störung regulatorischer Signaltransduktionskaskaden wird mit diversen Krankheiten assoziiert. Die Identifikation von regulatorischen Protein-Phosphorylierungsstellen stellt eine wichtige Rolle in der Erforschung von zellulären Signalweiterleitungsprozessen dar. Analysemethoden für das Phosphoproteom inkludieren meist Massenspektrometrie und ermöglichen die Identifikation von phosphorylierten Proteinen und Peptiden. Da Phosphopeptide meist in substöchiometrischen Mengen vorliegen, werden selektive Anreicherungsverfahren angewendet, welche die Sensitivität für phosphorylierte Peptidspezies erhöhen. Für die Optimierung einer phosphoproteomischen Analyse in Bezug auf Spezifität der Anreicherung, Robustheit und Effizienz des proteolytischen Verdaus wurden verschiedene proteolytische Verdau-Protokolle in Kombination mit titandioxid-basierter Affinitätschromatographie evaluiert. Die Evaluierung wurde anhand einer Perturbationsstudie mit einem Phorbolester als chemischen Trigger, angewendet in einem *in vitro* Jurkat Zellmodell, durchgeführt, um die der T-Zell Differenzierung zugrunde liegenden biologischen Mechanismen zu erforschen. Für die Evaluierung der Eignung von normalen proteomischen Analysen für die Identifikation von phosphorylierten Peptiden wurden die Ergebnisse des analysierten Phosphoproteoms gegen ein normales Proteom verglichen. Die Analyse der Proben wurde mittels moderner Ionenmobilitäts-Massenspektrometrie durchgeführt und durch die Aufnahme von Fluoreszenz-Zellbildern erweitert. Von den evaluierten Verdau-Protokollen wurden mit dem über Nacht-Verdau in Kombination mit der titandioxid-basierten Phosphopeptid-Anreicherung die meisten Peptide identifiziert. Es wurde ein Phosphopeptid-Anreicherungsfaktor von 98% erreicht, wobei 11,110 Phosphopeptide identifiziert wurden. 70% der identifizierten Phosphopeptide wurden als Klasse I Phosphopeptide klassifiziert. Wie erwartet wurden im normalen Proteom nur geringe Regulationen festgestellt, da die Phorbolester-Behandlungsdauer von drei Stunden keinen großen Einfluss auf die Proteinexpression hat. Die Phosphopeptid-Regulationen, welche phorbolester-bindende und endomembran-assoziierte Proteine beinhalteten, bestätigten die erfolgreiche Phorbolester-Behandlung. Die Fluoreszenz-Zellbilder zeigten Veränderungen im Endomembran Sytem und unterstützten die Ergebnisse der phosphoproteomischen Analyse. Die Annotation der identifizierten Phosphorylierungsstellen wurde via PhosphoSitePlus evaluiert und unterstrich die Notwendigkeit von funktionellen phosphoproteomischen

Analysen, da die Hälfte der Phosphorylierungsstellen entweder keine biologische Funktion aufwiesen oder gar keine Annotation gefunden werden konnte. Der optimierte Anreicherungsprozess erwies sich als wichtige Analysemethode, um eine umfassende Interpretation von zellulären Signalweiterleitungsprozessen in proteomischen Studien zu ermöglichen.

Graphical abstract

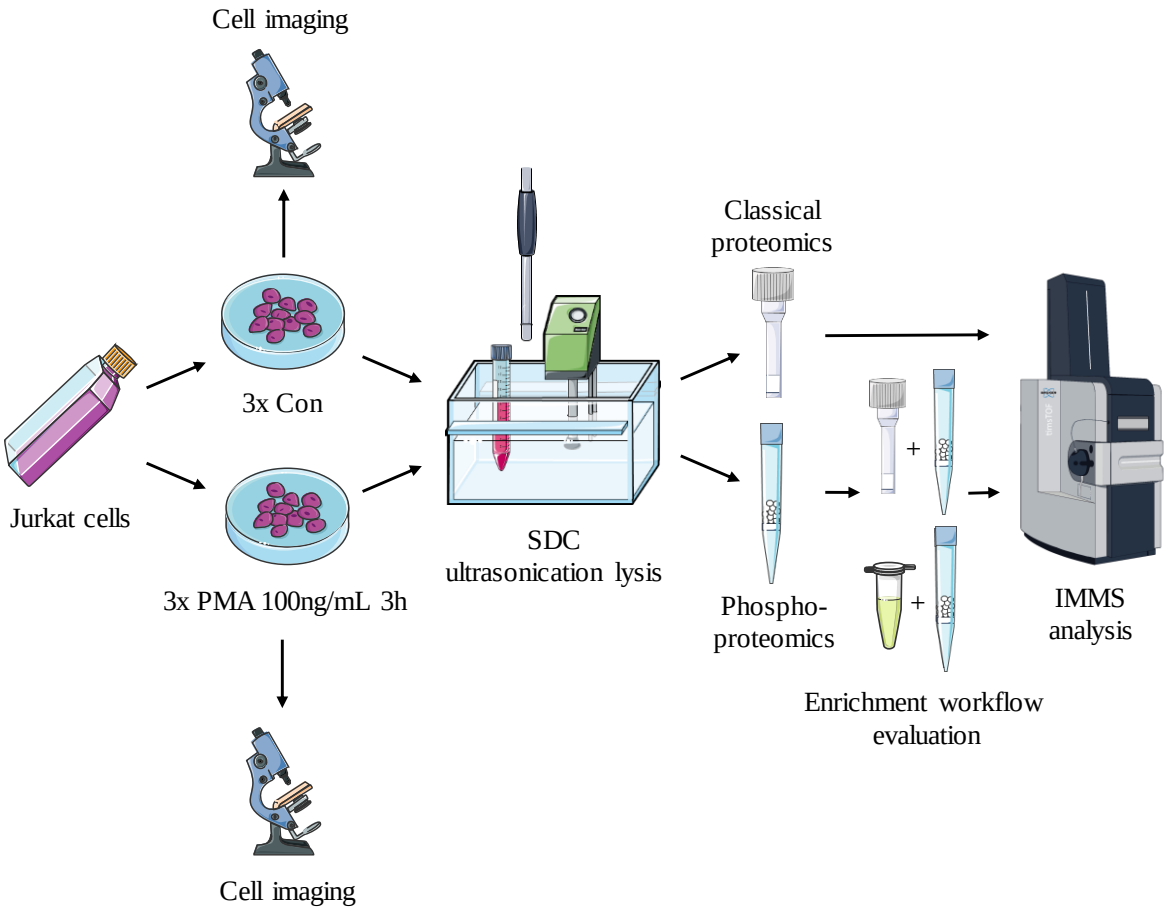

Figure 1 Schematic of the Master's thesis workflow. Jurkat cells were treated with PMA and undertaken a proteomic and phosphoproteomic analysis. Different phosphopeptide enrichment workflows were evaluated and samples were analyzed via ion mobility mass spectrometry. Additionally, fluorescence images of the Jurkat cells were taken [1].

Abbreviations

2-CAM	2-Chloroacetamide
ACN	Acetonitrile
ADP	Adenosine diphosphate
API	Atmospheric pressure ionization
APPI	Atmospheric pressure photo ionization
ATP	Adenosine triphosphate
BCA	Bicichoninic acid
BSA	Bovine serum albumin
CaMK	Ca^{2+}/calmodulin-dependent protein kinase
cAMP	Cyclic adenosine monophosphate
CCS	Collision cross section
CD	Cluster of differentiation
CDK	Cyclin-dependent kinases
CID	Collision- induced dissociation
CV	Coefficient of variation
DC	Direct current
DMSO	Dimethylsulfoxide
DTT	Dithiothreitol
EDTA	Ethylenediaminetetraacetic acid
EP	EasyPhos
ER	Endoplasmatic reticulum
ESI	Electrospray ionization
FA	Formic acid
FCS	Fetal calf serum
FDR	False discovery rate
FT-ICR	Fourier-transform ion cyclotron resonance
GMA	glycidyl methacrylate
HCD	Higher-energy collisional dissociation
HEPES	4-(2-hydroxyethyl)-1-piperazineethanesulfonic acid
HPLC	High performance liquid chromatography
IAA	Iodacetamide
IDA	Iminoacetic acid

IMAC	immobilized metal affinity chromatography
IMMS	Ion mobility mass spectrometry
IMS	Ion mobility spectrometry
IS	In-solution
IT	Ion trap
iTRAQ	Isobaric tags for relative and absolute quantitation
LB	Lysis buffer
LC	Liquid chromatography
LC-MS	Liquid chromatography mass spectrometry
LFQ	Label free quantification
MALDI	Matrix assisted laser desorption ionization
MAPK	Mitogen-acivated protein kinase
MCP	Multi-channel plate
MHC	Major histocompatibility complex
MOAC	Metal oxide affinity chromatography
MS	Mass spectrometry
MS/MS	Tandem mass spectrometry
NTA	Nitriloacetic acid
PASEF	Parallel accumulation- serial fragmentation
PBS	Phosphate buffered saline
PKC	Protein kinase C
PMA	Phorbol 12-myristate 13-acetate
pS	Phosphoserine
pT	Phosphotyrosine
PTM	Post-translational modification
RF field	Phosphotyrosine
Q	Quadrupole
QQQ	Triple Quadrupole
TOF	Time-of-flight
RF	Radio frequency
RSD	Relative standard deviation
SAX	Strong anion exchange
SCX	Strong cation exchange
SDC	Sodium deoxycholate

SDS	Sodium dodecyl sulfate
SILAC	Stable isotope labeling with amino acids in cell culture
TCEP	Tris(2-carboxyethyl)phosphine
TCR	T-cell receptor
TEAB	Triethylammonium bicarbonate
TFA	Trifluoroacetic acid
TIMS	Trapped ion mobility spectrometry
TMPTMA	trimethylol-propane trimethacrylate
TMT	Tandem mass tag
TOF	Time of flight
Tris-HCl	Tris(hydroxymethyl)aminomethan hydrochloride

1. Theoretical background

1.1. Mass spectrometry

Mass spectrometry is used for the determination of the mass-to-charge ratio of ionized molecules in the gas phase. In the field of proteomics, it enables the identification and quantification of peptides and proteins. In general, mass spectrometers consist of an ion source, a mass analyzer and a detector. [2]

Ionization methods include techniques such as electrospray-ionization (ESI) and matrix-assisted laser desorption/ionization (MALDI), both soft ionization techniques, with ESI being the most used and effective method in the field of proteomics. In ESI, small charged droplets are generated by passing the analyte solution through a small needle while applying a high potential, usually 2-5 kV, at atmospheric pressure. The application of an electric potential leads to a charge accumulation on the surface of the liquid, resulting in the formation of charged droplets with a diameter of approximately 5-60 µm. Evaporation causes the droplets to shrink, increasing their charge density and resulting in Coulomb explosions into smaller drops as soon as the Coulomb repulsion force exceeds the surface tension. When the droplets are small enough, the analyte ions are desorbed into the gas phase. The droplet formation is assisted by a nebulizer gas, usually nitrogen, helping to break the liquid into drops and acting as a drying gas at the entrance of the capillary. The efficiency of the ionization process can also be improved by adjusting the flow rate or the addition of organic solvents to the aqueous analyte solutions, which lowers the surface tension. In the case of proteomics, where the analyte solution usually contains peptides, the charge distribution of peptides increases with the length and number of ionizable moieties. The distribution of the charge states depends on the structure and the fold of the proteins in solution as well as pH, solvent composition, temperature and ionic strength. In proteomics, MS spectra are mostly acquired in the positive ionization mode with an acidified analyte solution, containing for example acetic acid or formic acid. [2]

The most common mass analyzers for proteomics are ion traps (IT), quadrupole mass filters (Q), time of flight instruments (TOF), Orbitrap analyzers and FT-ICR instruments. These mass analyzers are usually combined into hybrid instruments such as QQQ, Q-Orbitrap, Q-TOF or Q-ion mobility-TOF. [2]

1.1.1. Ion mobility mass spectrometry

The first ion mobility devices that were developed were drift tube devices. In drift tube ion mobility, the tube is filled with a stationary inert gas. An electric field is applied, forcing ions to drift through the tube. The velocity of drift v_d of the ion can be calculated by measuring the flight time through the drift tube, as the length of the drift tube is known. Resolving power in drift tube ion mobility devices can be improved by measuring the drift times accurately, therefore gating the ions into the drift tube with minimal time distribution is required. [3]

In ion mobility mass spectrometry hybrid instruments (IMMS), the MS is used as detection system. In IMMS, the interface between the IM and the MS part is critical. In the early stages of IMMS, the majority of the ions got lost at the interface to the MS, severely limiting sensitivity. In modern IMMS instruments, ion funnels and traps allow trapping and refocusing of the ions before injecting them into the MS analyzer, avoiding a loss of ions and enabling highly sensitive measurements. [3]

Consequently, a new generation of ion mobility devices was developed, implementing ion funnels into the drift tube analyzers. [3] This resulted in the introduction of RF ion confinement drift tubes [4], travelling wave based ion mobility [5] and several other techniques. In 2011, Park *et al.* developed the trapped ion mobility spectrometry (TIMS) [6]. In TIMS, ions are held stationary against a counter gas flow in the drift cell by applying an electrical field. This development allowed for a drastic reduction of the proportions of ion mobility analyzers, as in TIMS, ions are held stationary.

The steady state drift velocity v_d adopted by an ion can be calculated by multiplying the ion mobility K with the applied electric field E. (Equation 1)

Equation 1

$$v_d = K \cdot E$$

K describes the interaction of an ion with the drift gas, influenced by the shape and size of the ion as well as gas temperature, pressure, polarizability and composition. For simplifying the description of K, the reduced ion mobility K_0 can be used that standardizes K to standard temperature and standard pressure, T_0 and p_0. (Equation 2)

Equation 2

$$K_0 = K \cdot \frac{T_0}{T} \cdot \frac{p_0}{p}$$

In standalone IMS systems, K_0 is used to identify compounds by comparison with libraries. In IMMS instruments, the determination of K_0 by IM and m/z by MS can be used to identify the chemical species of an ion or to calculate its collision cross section (CCS) through Equation 3, a simplified version of the Mason Schamp equation, with *z* being the ion charge, *M* the ion mass and *m* the collision gas mass. The CCS is characteristic for the interaction between an ion and the drift gas.

Equation 3

$$CCS = 18500 \cdot \frac{z}{K_0} \cdot \sqrt{T \cdot \frac{M \cdot m}{M + m}}$$

The TIMS analyzer allows for a variety of methods, including sequential analysis, selected accumulation, parallel accumulation and gated TIMS. Ion sources for TIMS analyzers are atmospheric pressure ionization (API) sources such as ESI, nanoESI and APPI. Time-of-flight (TOF) and Fourier transform – ion cyclotron resonance (FT-ICR) mass analyzers have so far been used in IMMS devices, TOF analyzers having the advantage of their high scan speed and FT-ICR analyzers offering high mass resolutions. Between the TIMS analyzer and the MS analyzer, usually quadrupoles and collision cells are employed. [3] As sample analysis was performed on a timsTOF™ Pro (Bruker Daltonics Inc.) in this thesis, its structure will be described in detail.

1.1.2. timsTOF™

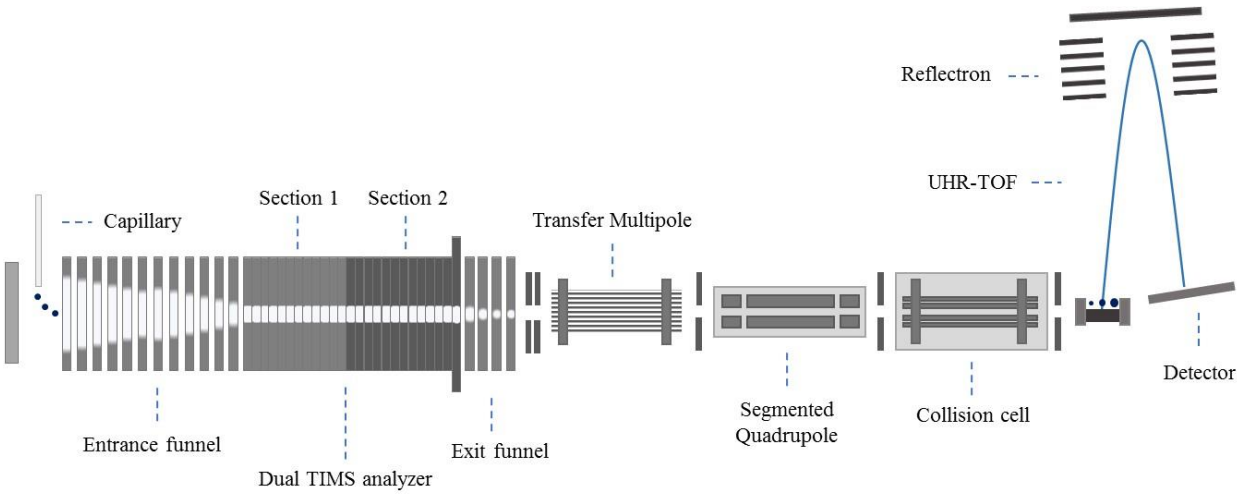

Figure 2 Structure of the timsTOF™ Pro.

The timsTOF™ Pro (Bruker Daltonics Inc.) is an IMMS instrument that combines a dual TIMS analyzer with an UHR-TOF (Figure 2). After ionization by the ESI source, desolvated ions enter the device through an orthogonal glass capillary, deflecting the ions by 90°. They are transferred into the dual TIMS analyzer through an electrodynamic double-focusing entrance funnel. The TIMS tunnel consists of stacked printed circuit boards (PCBs) with a length of 10 cm and a diameter of 8 mm, forming a stacked multipole. The trapped ions are radially confined by applying a RF potential. A gas flow pushes the injected ions forward in the TIMS analyzer with a force that is proportional to their CCS. From the entrance to the exit, an increasing longitudinal DC field gradient is superimposed on the applied RF field. As a result, the ions are dragged forward by the gas flow and repulsed by the counteracting electrical field. Depending on their CCS values and charge states, ions are held at the point where the force of the gas flow and the counteracting electrical field are equal. As the drag of the gas flow is proportional to the CCS of an ion, ions are trapped at different positions along the TIMS tunnel, with high mobility ions coming to rest closer to the entrance, and low mobility ions closer to the exit. After a defined accumulation time, the entrance of further ions is prevented by changing the potential of the deflection plate. Separation of the stored ions based on their ion mobility is achieved by ramping the potential of the second TIMS section. While the ion mobility based separation and analysis takes place in the second section of the TIMS tunnel, new ions can be collected in the first section, storing and pre-separating ions according to their

ion mobility. The parallel accumulation and analysis in the dual TIMS analyzer enables overall duty cycles up to 100% with usual accumulation and ramp times of 50-200 ms. Different ion mobility resolution modes can be selected in order to investigate a wide mass range or maximize ion mobility resolution for peaks of special interest. The stored ions are released from the TIMS analyzer by linearly decreasing the electric field gradient. Low mobility ions are eluted before highly mobile ions, having a smaller collision cross section in relation to their charge. The released ions pass through a focusing exit funnel towards a transfer multipole and enter the segmented quadrupole, in which m/z values for precursor ion selection can be filtered (MS/MS scan). In the collision cell, ions are accelerated and either fragmented by collision with an inert gas (MS/MS scan) or further transferred without fragmentation (MS scan). The ions are pushed into the orthogonal accelerator unit, ion packages are formed and ejected into the drift tube. In the drift tube, mass analysis is performed under field free conditions. The ions perform a V-shaped flight path, are reflected by a two-stage reflectron that compensates for kinetic energy distributions of the ions and are detected by a multi-channel plate ion detector (MCP). The addition of ion mobility as an additional separation dimension allows for the differentiation of isomeric and isobaric compounds. After separation of the compounds and fragmentation, this results in clean MS/MS spectra. Deflecting the ions by 90° at the entrance of the device and an improved quadrupole design increase the robustness of the device. In addition to high mass resolution of up to 200, the timsTOF™ provides high mass accuracy in the low ppm range. The combination of accurate CCS values (<0.5 % RSD) and clean MS/MS fragmentation spectra offers high specificity. [7, 8]

1.2. Proteomics

The term of proteomics was first used in 1995 by Marc Wilkins to describe "the protein complement of the genome" [9] and is commonly used for the description of the large-scale analysis of proteomes. A proteome is defined as the entirety of proteins in a given organism, cell, or tissue in a defined state at a specific time point. Proteomic analyses include the identification and quantification of primary and secondary protein structures, protein conformations, post-translationally modified proteins, protein isoforms, alternative protein splice forms and polymorphisms. It facilitates the cellular localization of proteins, the determination of their turnover rates in dependence of external stimuli, time and cell type. Proteomic approaches can be classified into top-down, middle-down and bottom-up techniques. Top-down proteomics is an approach for the analysis of intact proteins, usually employing electron collision dissociation or electron transfer dissociation. Compared to the other approaches, top-down methods exhibit more difficulties in terms of protein fractionation, ionization and fragmentation, but are more suitable for the localization of PTMs and identification of protein isoforms. Middle-down proteomic workflows employ the partial proteolytic digest of proteins and analyze the resulting large peptides. Bottom-up proteomics, also known as shotgun proteomics, is used for the identification of proteins through analysis of their peptides by tandem mass spectrometry. [10]

In the beginnings of shotgun-proteomics, two-dimensional gel electrophoresis was used for the separation of protein mixtures based on their isoelectric point and molecular weight. Protein spots were punched out, enzymatically digested and subsequently identified via mass spectrometry, giving insights into the networks of biological systems. The implementation of electrophoretic fractionation, enzymatic digestion and mass spectrometric analysis is described by the term of peptide mass fingerprinting and was developed independently by several researchers in 1993. [11–13]

In peptide mass fingerprinting, m/z values of peptides are determined by mass spectrometry. As the masses of amino acids and the cleavage sites of proteolytic enzymes are known, an *in-silico* digest of proteins, e.g. the human proteome, can be performed, yielding in the masses of all theoretically resulting peptides. Search algorithms are then used to assign experimentally obtained m/z values and spectra to peptide candidates by comparing them to the theoretical masses and spectra in public repositories such as UniProt. Ideally, this results in peptide spectrum matches, in turn enabling the identification of proteins. [14]

Since the early days of shotgun proteomics, proteomic workflows underwent continuous improvement to enable the large-scale analysis of proteins in complex matrices, including improvements in enzymatic digest, fractionation of peptides by liquid chromatography, employing the use of tandem mass spectrometry and developing bioinformatic tools for data interpretation. The demand for mass spectrometers with high sensitivity, accuracy and resolution evolved. The employment of new MS technologies enabled the development of new proteomic techniques such as multidimensional protein identification, PTM identification and protein quantification, including labelled and label-free approaches. [10] These evolutions made proteomics an important tool for molecular, cellular and systems biology, being able to investigate protein interactions, cellular signaling pathways and therefore being a powerful tool for the investigation of several diseases and identification of drug targets [15].

1.2.1. Phosphoproteomics

The analysis of the phosphoproteome is crucial for gaining better insights into the regulatory pathways of protein phosphorylation and dephosphorylation, which play major roles in several diseases. Mass spectrometry offers several advantages for the investigation of protein phosphorylation, facilitating its highly sensitive analysis and quantitative as well as site-specific measurements. These opportunities lead to the emergence of the field of phosphoproteomics, the large scale study of protein phosphorylation, at the turn of the century. [16] PhosphoSitePlus, the largest phosphoproteomic MS-database, currently contains 293,499 non-redundant serine, threonine and tyrosine phosphorylation sites [17], but only approximately 30% of these sites have been identified in more than one MS-based experiment [16]. 95% of identified human phosphosites have no reported biological function or kinase and only 20% of kinases phosphorylate 87% of currently annotated substrates. These numbers illuminate the scale of the phosphoproteome and that a vast part of it is still completely unexplored, highlighting the opportunity for further investigation of cell signaling pathways using phosphoproteomics. [16]

1.2.1.1. Challenges in phosphoproteomics

Protein phosphorylation and dephosphorylation are fast, highly dynamic cascade processes. Capturing the phosphorylation and dephosphorylation events happening upon a specific perturbation in *in vitro* or even *in vivo* models and furthermore correctly interpreting them can be hindered by several difficulties in phosphoproteomic approaches. [18]

In many studies, large amounts of protein are used as starting material, leading to the identification of large numbers of phosphorylation sites, but information about the stoichiometry is often missing. It is often not taken into consideration how many of the observed phosphorylation events are randomly occurring without any functional consequence and how many are the results or triggers of specific events. [18] Phosphatase inhibitors are commonly used in phosphoproteomic workflows during cells lysis to prevent protein dephosphorylation during sample preparation. While this approach enables the identification of high numbers of phosphorylation sites, it gives rise to the question whether the inhibition of phosphatases could also lead to hyperphosphorylations. Such hyperphosphorylations would not naturally occur in cells under physiological conditions at an abundance that makes them analyzable by phosphoproteomics. [16] Humphrey *et al.* inactivate phosphatases and proteases by heat treatment during cell lysis in their EasyPhos workflow because different phosphatase/protease inhibitors inhibit different enzymes, leading to the detection of distinct phosphorylation sites [19]. Thingholm *et al.* found that the treatment of cells with distinct phosphatase inhibitors (Calyculin A, sodium pervanadate, phosphatase inhibitor cocktail) increases the number of identified phosphopeptides by 10-40% and significantly effects the distribution of phosphorylation sites. This increase in identified phosphorylation sites might reflect secondary hyperphosphorylation events due to the inhibition of phosphatases, which would otherwise dephosphorylate the responsible upstream kinases. [20] Pan et al. compared cells treated with a phosphatase inhibitor mix to a control group using SILAC and detected an unequal inhibitory effect on different phosphosites. Effectively inhibiting tyrosine phosphorylation, only half of the serine and threonine phosphoproteome was affected by the phosphatase inhibitor mix. [21]

Even if phosphorylation sites are correctly conserved during cell lysis and sample preparation steps, it has to be taken into account that not all phosphorylation sites in an organism are phosphorylated at the same time, as phosphosites are context-dependently regulated. Many phosphosites are modified or unmodified at different stages of the cell cycle. Perturbations performed e.g. on a cell culture model are likely to cause phosphorylation and dephosphorylation events in a time-dependent manner, highlighting the need for temporal

profiling of phosphorylation events in such studies. Kinetic studies employed in phosphoproteomics could also shed light on cellular cascade processes. [18, 22]

Reduced digestion efficiency is frequently observed for phosphorylated proteins. Trypsin is the most commonly used protease in proteomic studies due to its high specificity and effectiveness. However, in the case of phosphoproteomics, the proteolytic cleavage of phosphopeptides is often impaired by phosphate residues, resulting in a higher number of missed cleavages. The impairment depends on the position of the phosphorylated amino acid, as well as the type of amino acid. [18] For trypsin and Lys-C, phosphoresidues in the positions +1, +2 and +3 are most likely to impair proteolytic cleavage [23, 24]. It is recommended to optimize digestion conditions, for example using high concentrations of enzyme (1:20 (w/w) enzyme to protein ratio) to improve digestion efficiency and prevent sensitivity loss. Reduced digestion efficiency can particularly impair quantitative phosphoproteomic approaches using SILAC, as digestion efficiency can be up to 10 times more efficient for non-phosphorylated peptides in comparison to their phosphorylated form. [18] The coverage of the phosphoproteome can also be extended by the use of alternative proteases. Giansanti *et al.* compared five different proteases (AspN, chymotrypsin, GluC, LysC, trypsin) in a phosphoproteomic approach. As expected, trypsin clearly outperformed the other proteases in the number of identified phosphorylation sites, but the obtained phosphoproteomic data sets using different proteases were highly complementary to each other. Only about one third of all identified phosphosites were identified in more than one dataset. The use of alternative proteases might be especially useful for the specific investigation of regulatory phosphorylation sites on signaling proteins that play a major role in signaling pathways. [23]

Phosphopeptides show high affinity to metal ions and metal oxides. [25, 26] This property is frequently used in IMAC and MOAC workflows for phosphopeptide enrichment, but can lead to phosphopeptide loss during sample preparation and LC-MS analysis, as many surfaces are metals, such as syringes and ultrasonication devices for cells lysis and HPLC flow paths [18]. The addition of additives such as EDTA or citrate to LC buffers can decrease the absorption of phosphopeptides to metal surfaces of the HPLC flow path [27]. For cell lysis, using strategies that do not require contact of the sample with metal surfaces might decrease sample loss [18].

Compared to their non-phosphorylated counterparts, phosphopeptides sometimes show reduced ionization efficiency that increases with the number of phosphorylation sites [18]. Concerning the fragmentation behavior of phosphopeptides, their labile phosphoester bond can impair fragmentation. The low-energy pathway of fragmentation of the phosphoester bond can

compete against the usual fragmentation of the amide bond along the backbone of the peptide. Depending on the used fragmentation type, neutral loss of H_3PO_4 or HPO_3 from the precursor ion can occur which can decrease spectrum quality, complicate spectrum identification and impair phosphosite localization. Especially in CID, the labile phosphoester bond tends to break first, whereas HCD- type fragmentation provides better performance for phosphoproteomic experiments. Serine phosphorylated peptides usually show a dominant loss of H_3PO_4, whereas threonine phosphorylated peptides show more HPO_3 fragments and tyrosine phosphorylated peptides exhibit less neutral losses in general, predominantly being HPO_3. [18, 28] Due to poor quality spectra including dominant neutral losses, phosphorylation localization algorithms such as the A-score [29], the Mascot Delta Score [30] and the PTM score of MaxQuant [31] can mislocalize the phosphate residue within a given peptide sequence. [18]

Phosphorylated proteins are generally present at substoichiometric abundance in comparison to their non-phosphorylated counterparts. Therefore, phosphopeptide enrichment steps usually need to be employed into phosphoproteomic workflows to enable the identification of high numbers of phosphopeptides and -proteins. [18]

1.2.1.2. Phosphopeptide enrichment strategies

One of the first strategies used for phosphopeptide enrichment were metal based strategies, including the immobilized metal affinity chromatography (IMAC) and the metal oxide affinity chromatography (MOAC). In IMAC, metal ions are immobilized on a solid matrix (beads) through chelators. The phosphopeptide enrichment mechanism is based on the affinity of phosphate groups to metal ions. [26] The first adsorbents that were developed consisted of iminoacetic acid (IDA) or nitriloacetic acid (NTA) as chelators in combination with Fe^{3+} and Ga^{3+} as metal ions [32]. Due to the affinity of these traditional IMAC materials to acidic non-phosphopeptides, they exhibited insufficient specificity. Novel IMAC materials were developed, using Ti^{4+} and Zr^{4+} with the flexible linker poly(GMA-co-TMPTMA), resulting in a high selectivity for phosphopeptides, comparable to that of MOAC and improving the drawbacks of the traditional adsorbents. [33, 34] As all metal ions have different binding affinities to acidic, basic, mono- and multi phosphorylated peptides, combining different metal ions into a sequential enrichment workflow might also improve enrichment efficiency [26].

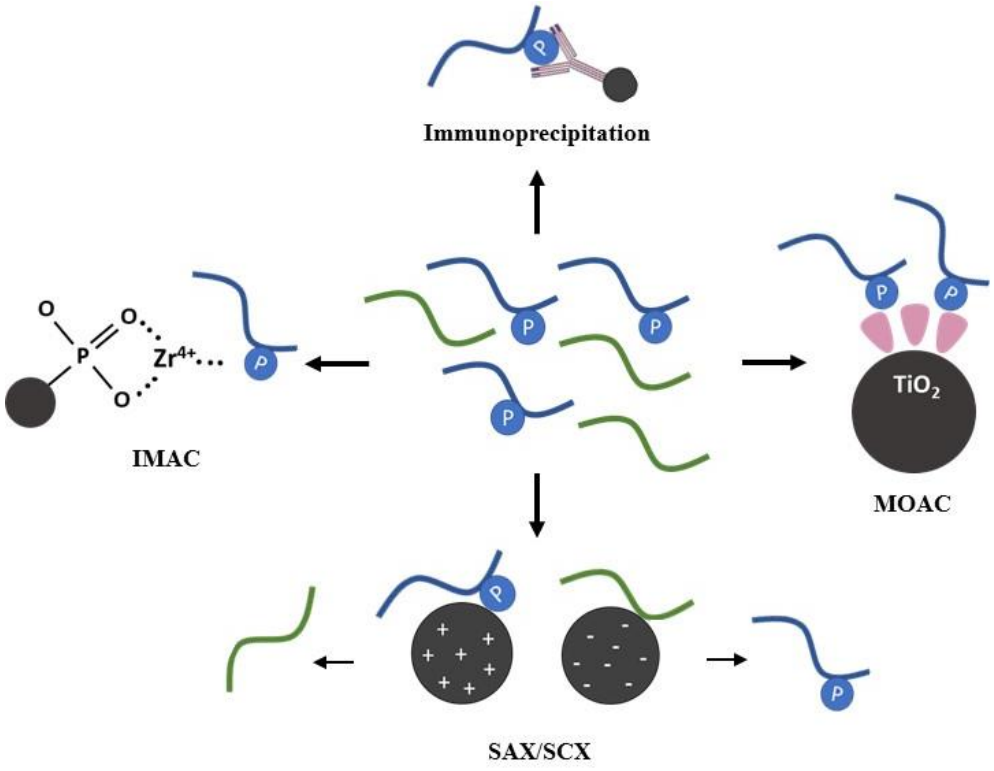

Figure 3 Schematic overview of different phosphopeptide enrichment strategies. IMAC and MOAC are the most common approaches for general phosphoproteomic workflows, while immunoprecipitation is mainly used for specific enrichment of tyrosine-phosphorylated peptides. SAX and SCX might be used for pre-fractionation of phosphopeptides [1].

In MOAC, metal oxides are used for the selective enrichment of phosphopeptides. Phosphate groups exhibit high affinity to metal oxides, binding to their surface in a bidentate manner. Metal oxides are lewis acids and the extraction mechanism is based on lewis acid–base interactions, with each metal oxide exhibiting a different acidity contributing to different selectivities. [35] The first metal oxide that was used for phosphopeptide enrichment was TiO_2, followed by the development of many more, such as ZrO_2, $Al(OH)_3$, Ga_2O_3, Fe_3O_4, SnO_2 and HfO_2. Again, the selectivity of metal oxides differs, compared to TiO_2, ZrO_2 shows higher selectivity for monophosphopeptides, whereas Fe_3O_4 has a higher affinity to multi-phosphorylated peptides. Compared to IMAC, MOAC workflows are usually more robust, as MOAC materials less sensitive to detergents and buffers. Similar to IMAC, the combination of different MOAC materials can be used to further improve enrichment specificity. [26] For example, TiO_2-ZrO_2 monodisperse microspheres exhibit improved enrichment specificity in comparison to single metal TiO_2 [36]. Although composite materials show promising advantages in comparison to single metal oxides, and selectivities of metal oxides vary greatly, TiO_2 remains the most widely used metal oxide for phosphopeptide enrichment due to its commercial availability and high specificity [35]. Workflows using TiO_2 based MOAC are being constantly improved by optimizing extraction conditions. Performing phosphopeptide enrichment at low pH protonates acidic residues such as glutamic and aspartic acid, reducing their binding to MOAC and IMAC beads. [26]

Besides metal-based enrichment strategies, immunoprecipitation is a highly efficient and specific phosphopeptide enrichment method. Immunoprecipitation employs antibodies binding to phosphorylated amino acids. Rather than being a suitable enrichment strategy for large-scale phosphoproteomic studies, immunoprecipitation can be used to improve the enrichment sensitivity towards certain phosphopeptides, mainly tyrosine-phosphorylated peptides. Tyrosine phosphorylation occurs at substoichiometric abundance on a cellular level, leading to an underrepresentation of tyrosine-phosphorylated peptides in common IMAC or MOAC enrichment workflows. As antibody-based approaches are expensive and the availability of antibodies is limited, especially for serine- and threonine phosphorylated peptides, this strategy hasn’t been employed as extensively as metal-based strategies in phosphoproteomic studies yet. [25, 26]

Ion exchange chromatography methods consist of strong anion exchange chromatography (SAX) and strong cation exchange chromatography (SCX). This enrichment method is based on the charge difference between phosphopeptides and non-phosphopeptides. SCX consists of

a negatively charged solid phase and an acidic buffer as mobile phase. At low pH, lysine and arginine residues and the N-terminal amino groups of peptides are protonated. Tryptic peptides contain C-terminal arginine or lysine residues, therefore the majority of non-phosphopeptides exhibit a net charge of +2, whereas mono-phosphorylated peptides have a net charge of +1. Due to the additional phosphate groups, multi-phosphorylated peptides are not retained by SCX and get lost in the flow-through. Bound peptides are gradually eluted by increasing the pH and/or iconic strength of the buffer. SAX contains a positively charged matrix and a neutral or alkaline buffer. At high pH, peptides have a negative net charge, as lysine and arginine residues are uncharged and the C-terminal carboxyl group, aspartate and glutamate are single-negatively charged. Phosphopeptides bind to the matrix due to their negative charge and are eluted later than non-phosphopeptides. Ion exchange chromatography cannot distinguish phosphopeptides from non-phosphopeptides with the same net charge, hence it is usually used for the pre-fractionation of phosphopeptides rather than direct enrichment. [25] The pre-fractionation by ion exchange chromatography can improve the relative abundance of phosphopeptides in complex peptide samples, increasing the efficiency of following enrichment steps. [25, 26]

MOAC and IMAC are still the most efficient and commonly used phosphopeptide enrichment strategies. SCX and SAX are more suitable for pre-fractionation of phosphopeptides rather than direct enrichment and immunoprecipitation is the method of choice for specific phosphotyrosine enrichment. [26]

1.2.2. Labeling strategies

In order to determine peptide and therefore protein abundances, several quantitative proteomic methods have been developed that can be equally applied to phosphoproteomics. Quantitative approaches include label-free quantification methods, stable isotope tagging and targeted quantification techniques. The application of quantitative methods to phosphoproteomics is especially useful as protein phosphorylation changes can be determined, for example in kinetic studies. Proteomic labeling approaches include two main groups. Metabolic labeling uses techniques such as SILAC (stable isotope labeling with amino acids in cell culture), while chemical labeling strategies include iTRAQ (isobaric tags for relative and absolute quantification) and TMT (tandem mass tags). [37]

When applying SILAC labeling, cells are cultured in cell culture medium containing either heavy or light isotope labeled amino acids which are metabolically incorporated into the expressed proteins. Cells or protein extracts of the different conditions are then mixed in equal proportions, enzymatically digested and analyzed via LC-MS/MS in a single sample. Peptides of each condition are distinguished by the mass shift derived from the isotope labels, as the ratio of the intensities between the variants corresponds to the difference of their abundance. The analysis of both conditions in one sample allows for highly reproducible and accurate protein identification and relative quantification. [10]

In LFQ, individually prepared samples are analyzed separately. As differences in sample preparation can lead to inaccurate quantification, minimum and reproducible sample preparation is crucial for LFQ approaches. [10] In LFQ, different approaches are used for determination of protein abundance, including spectral counting of MS/MS spectra of a peptide, extraction of precursor ion intensity or summation fragment ions from MS/MS. Normalization methods for label free quantification can be based on the intensity between runs, the number of expected peptides from a certain protein or the difference in ionization efficiency of the peptides. [2, 38]

iTRAQ and TMT tags consist of a peptide reactive group, that covalently attaches the label to the peptide, a mass balancer group making each tag isobaric and a cleavable reporter group with a specific mass for peptide quantification. iTRAQ and TMT labelling is based on the same principle, but the labels differ in the structure of their equilibrium group. In both techniques, the reporter groups are mass matched with their balancer groups, resulting in different isoforms with equal masses. The reporter groups are released from tagged peptides during MS/MS

fragmentation, allowing for peptide and therefore protein abundance comparison between samples. [37] One major drawback of iTRAQ and TMT-labeling approaches is the possible co-isolation of ions with similar elution times and m/z-values during LC-MS/MS analysis, resulting in wrong quantification ratios and low accuracy. As this phenomenon tends to compress ratios towards one, it is often referred to as “ratio compression”. [37, 39]

When comparing LFQ, SILAC and MS2-/MS3- based TMT labeling in a quantitative phosphoproteomic approach, Hogrebe *et al.* found that SILAC and LFQ resulted in the most accurate results. Although the results based on MS2-TMT-labeling exhibited the highest precision, they showed the lowest accuracy due to ratio compression. MS3-based TMT-labeling partly overcame these drawbacks and showed higher accuracy. When comparing MS2- and MS3- based TMT-labeling, the results indicated that the MS2- approach is more suitable for the quantitative phosphoproteomics analysis of complex biological samples, while the high accuracy of MS3-based TMT labeling enables the determination of phosphorylation site stoichiometry. In general, SILAC and LFQ were found to be more accurate than TMT-labeling. [40]

1.3. Protein phosphorylation

1.3.1. Biochemistry of protein phosphorylation

Protein phosphorylation is a reversible posttranslational modification regulated by kinases and phosphatases [41]. It mainly occurs on the amino acids serine, threonine and tyrosine, in relative abundances of approximately 90%, 10% and 0.05% [42] and is the most widespread posttranslational protein modification. Approximately 10-30% of the human proteome are phosphorylated [43]. Protein kinases catalyze the transfer of a gamma-phosphoryl group to a hydroxyl group of specific amino acid residues on proteins, using ATP as a donor. Protein kinases consist of two main groups, the serine/threonine kinases and the tyrosine kinases. These two groups can be further divided into several families according to the structure of their kinase domain, their substrate specificity and the type of their regulation and activation. The catalytic activity of kinases is activated through the phosphorylation of residues in their catalytic domain, the activation loop, which usually consists of 200-300 amino acids. Most kinases are activated by another kinase, forming the center of the signaling cascade. Apart from phosphorylation by a kinase kinase, the presence of a second messenger intermediate can be required for kinase activation. Such second messengers are usually small molecules such as lipids, cyclic adenosine monophosphate (cAMP) and calcium.

The substrate specificity of kinases is determined by several factors, one being the type of residues next to the phosphoryl group acceptor. For example, kinase members of the CaMK and AGC group usually catalyze the phosphorylation of amino acids next to basic amino acids such as lysine and arginine, whereas kinases of the CDK, MAPK and CMGC groups usually phosphorylate residues near proline. Docking domains, also referred to as docking motifs, both on the kinase and the substrate, further increase the substrate specificity. These docking sites are usually located far away from the catalytic domain of the kinase and from the acceptor site on the substrate.

Protein phosphatases catalyze the transfer of a phosphoryl group from a protein to ADP as acceptor. Just like protein kinases, protein phosphatases are grouped into serine/threonine phosphatases, which are again split into the PPP and PPM family, and tyrosine phosphatases, containing the PTP phosphatases. The eukaryotic genome encodes for a larger number of kinases than for phosphatases. [41]

1.3.2. Biological function of protein phosphorylation

The phosphorylation of a protein changes its surface charge distribution, conformation and many more properties, therefore influencing protein-protein interactions and enzymatic activities. Protein phosphorylation and dephosphorylation are key regulatory processes in cellular signaling, with protein kinases and phosphatases being critical signal transducers, and influencing almost all cellular processes, such as cell metabolism, cell proliferation, apoptosis and extracellular signaling. [44] The regulation of protein phosphorylation is a highly complicated cascade process and the dysregulation of its regulatory pathways is commonly associated with different diseases, such as cancer [45, 46], neurological diseases [47], diabetes [48, 49], immune and infectious diseases [50]. As kinases play a crucial role in the carcinogenesis in different cancers, they are often the drug targets of cancer therapies. In 2018, kinase inhibitors accounted for approximately a quarter of all drug research efforts, mostly targeting tyrosine kinases [45]. The identification of phosphorylation sites is crucial for a better understanding of cellular signaling and helps to draw conclusions in disease-involved enzymes and phosphorylation sites [44].

1.4. T-cells

T-cells (T-lymphocytes) are a central component of the human adaptive immune system, playing a crucial role in immune response to pathogens, yet being responsible for the pathogenesis of several autoimmune diseases. T-cells originate as precursor cells from the bone marrow and mature in the thymus where key aspects of their responsiveness are set through a complex series of differentiation steps. Therefore, studying T-cell development and differentiation can give insights into their functions. T-cells can be classified into two major classes which differ by the expression of CD4 or CD8 glycoproteins on their surfaces. The CD (cluster of differentiation) molecules are responsible for the binding of major histocompatibility complex (MHC) molecules on antigen-presenting cells and T-cell receptor (TCR) signaling. CD4 assists the TCR by binding to MHC class II peptide complexes, whereas the CD8 coreceptor binds to MHC class I complexes. Activation of CD8+ T-cells differentiates them into cytotoxic effectors, while CD4+ T-cells have a wider functional potential, often referred to as helper T-cells. [41, 51, 52]

1.4.1. T-cell *in vitro* systems

Although the limitations of *in vitro* studies are known and *in vivo* studies using mouse models for the investigation of T-cell development have gained popularity in the twenty-first century, cell culture studies using T-cell lines still offer many advantages. The development knockout and transgenic mice is very time and resource consuming and not suitable for many studies. Moreover, germline gene disruptions involving signaling proteins can cause blocks in the development of T-cells. This can complicate the functional investigation of protein targets in antigen-responsive T-cells. Furthermore, the mouse immune system mostly parallels the human immune system, but the study of T-cell development in patients with immunodeficiencies might be inapproachable. For example, Zap $70^{-/-}$ mice contain no peripheral CD4+ T-cells, whereas these cells are abundant in Zap70 deficient humans. In summary, *in vivo* approaches for the functional investigation of proteins involved in T-cell signaling are indisputable, but *in vitro* experiments with T-cells complement the disadvantages of mouse models. [53]

1.4.2. Jurkat cells

The Jurkat cell line is a human t-cell lymphocyte cell line that was isolated from the peripheral blood of a 14-year old boy with T-cell leukemia in 1977 [54]. *In vitro* studies employing Jurkat cells were the foundation of T-cell receptor signaling research and contributed to the mapping of many signaling pathways [53].

1.4.3. PMA

Phorbol-12-myristate-13-acetate (PMA) specifically activates protein kinase C (PKC) and results in activation of the transcription factor NF-κB [55]. NF-κB is involved in the pathogenesis of different diseases and is a therapeutic target of inflammatory processes, autoimmune diseases and cancer. [56]

2. Aims & objectives

The aim of this master's thesis was the evaluation of different workflows for phosphopeptide enrichment including metal oxide affinity chromatography. The evaluation was performed using an *in vitro* cell line model, performing a perturbation study with PMA as a chemical trigger. Sample analysis was performed employing "state-of-the-art" ion mobility mass spectrometry. Evaluation parameters were based on phosphopeptide enrichment specificity, robustness and proteolytic digestion efficiency of the different workflows. Results from the obtained phosphoproteome experiments were compared against the background proteome in order to obtain functional insights into biological mechanisms driving differentiation of T-lymphocytes. Additionally, the biological interpretation of the obtained results was strongly supported by fluorescence cell imaging. A schematic of the master's thesis workflow can be found in Figure 1 in the graphical abstract.

3. Materials and Methods

3.1. Cell culture

Jurkat cells (ATCC® TIB-152™) were thawed, transferred to a 15 mL Falcon tube, 5 mL cell culture medium (RPMI-1640) supplemented with 10% (v/v) heat inactivated FCS (Sigma Aldrich, 56°C for 30 min) and 1% (v/v) penicillium/streptomycin (Sigma Aldrich 1000U Penicillium, 10mg/ml Streptomycin) were added and centrifuged at 220 x g for 5 minutes (Heraeus™ Megafuge™ 16R, Thermo Scientific). The supernatant was discarded, the cell pellet was resuspended in 1 mL preheated cell culture medium (37°C) and transferred into 19 mL preheated cell culture medium in a T75 cell culture flask. The cells were incubated at 37°C, 5% CO_2 (Heracell 150i CO_2 Incubator, Thermo Scientific). For splitting the cells, they were transferred to a Falcon tube, centrifuged at 220 x g for 5 minutes, the supernatant was discarded and the cell pellet was resuspended in 2 mL preheated cell culture medium. 19 mL preheated cell culture medium were added to the previously used T75 cell culture flask and 19 mL were added to a new T75 cell culture flask. 1 mL of the resuspended cells were added to each cell culture flask and the cells were again incubated at 37°C, 5% CO_2. The cells were cultured until nine T75 cell culture flasks with approximately 50,000 cells each, yielding approximately 450,000 cells in total, were obtained, cell culture medium was changed as described every 4-5 days.

3.1.1. Cell imaging

Cells from one flask were separated from the medium by sedimentation (200 µL concentrated cell suspension from original 1000 µL) and stained with 500 µL staining solution (ER Staining Kit Cytopainter, Abcam and CellMask™ Deep Red Plasma membrane stain, Thermo Fisher Scientific) for 15 min. The ER staining solution was diluted 1:1000, the membrane stain 1:2000. After the incubation, the cell suspension was divided into 2 identical aliquots, washed with pre-warmed live cell imaging solution and resuspended in a total volume of 300 µL live cell imaging solution. For PMA treatment, a PMA stock solution (1 mg/mL in DMSO) was first diluted 1:1000 with cell culture medium and then 1:100 in live cell imaging solution, giving a final concentration of 10 ng/mL. As a solvent control, controls were treated with DMSO (conc.) diluted equally. Cells were seeded in a µ-Slide $VI^{0.1}$ Ibitreat and imaged after 30 and 60 min incubation with a C-Apochromat 63X/1.2 W KorrM27 objective (Zoom 2) at a wavelength of 488 nm for the ER stain and at 647 nm for the plasma membrane stain.

3.1.2. PMA treatment

For PMA treatment, the cell culture medium of the remaining eight cell culture flasks was changed as described previously. The cells of four flasks were then cultured with cell culture medium with 100 ng/mL PMA ("Jurkat PMA") and the other four flasks with cell culture medium without any additives ("Jurkat Con"). The cells were incubated at 37°C, 5% CO_2 for 3 hours.

3.1.3. Cell lysis

The cells were transferred into falcon tubes and centrifuged at 220 x g for 5 minutes. The supernatant was discarded, the cells were washed by resuspending the cell pellet in 5 mL PBS and centrifuged again at 220 x g for 5 minutes. The procedure was continued once more. The supernatant was discarded and the cells pellets were stored on ice. 100 µL of precooled SDC lysis buffer (4% (w/v) SDC, 100 mM Tris-HCl, pH 8.5) were added to three cell pellets of each condition and 100 µL hypotonic lysis buffer (10 mM HEPES/NaOH, pH 7.4, 0.25 M sucrose, 10mM NaCl, 3mM $MgCl_2$, 0.5% Triton X-100) were added to one cell pellet of each condition. The suspensions were immediately heat-treated for 5 minutes at 95°C in a water bath. The lysates were cooled to room temperature, homogenized via ultrasonication (Sonoplus HD 2070, Bandelin) and stored at 4°C overnight.

3.2. Sample preparation

To remove insoluble matter, cell lysates were centrifuged at 700 x g for 10 minutes, supernatants were transferred into Eppendorf tubes and centrifuged at 13,000 x g for 5 minutes (Fisherbrand™ accuSpin™ Micro 17 Microcentrifuge, Fisher Scientific). The supernatants were again transferred into new Eppendorf tubes and the samples that were lysed using SDC lysis buffer were pooled. BCA-assay was performed to determine protein concentrations.

3.2.1. BCA assay

In a 96 well plate, calibration standards were prepared by diluting 1-5 µL 1 µg/µL BSA with LC-MS grade water and SDC lysis buffer or Protifi® lysis buffer (8 M Urea, 50 mM TEAB, 5% (v/v) SDS, pH 7.55) to a total volume of 10 µL. Samples were diluted by mixing 1 µL sample with 9 µL LC-MS grade water. BCA working reagent was prepared immediately before use by mixing 5 mL reagent A (26 mM bicinchoninic acid disodium salt hydrate, 186 mM sodium carbonate, 8 mM sodium tartrate, 113 mM sodium bicarbonate, pH 11.25) with 0.1 mL reagent B (200 mM copper sulfate pentahydrate). 200 µL BCA working reagent were added to

each well, the plate was incubated at room temperature at 900 rpm on a shaker for 1 minute in the dark, followed by incubation at 60°C for 30 minutes in the dark. Absorbance was measured at a wavelength of 562 nm (Multiskan™ GO Microplate Spectrophotometer, Thermo Scientific™). For the samples lysed with SDC-buffer, protein concentrations of 1.98 µg/µL (Jurkat Con) and 1.20µg/µL (Jurkat PMA) were determined, for the samples lysed with hypotonic buffer protein concentrations of 4.46 µg/µL (Jurkat Con) and 4.55 µg/µL (Jurkat PMA) were obtained.

3.3. Proteomics and phosphoproteomic enrichment strategies

For further processing and the implementation of different proteolytic digestions protocols, samples were divided according to Figure 4.

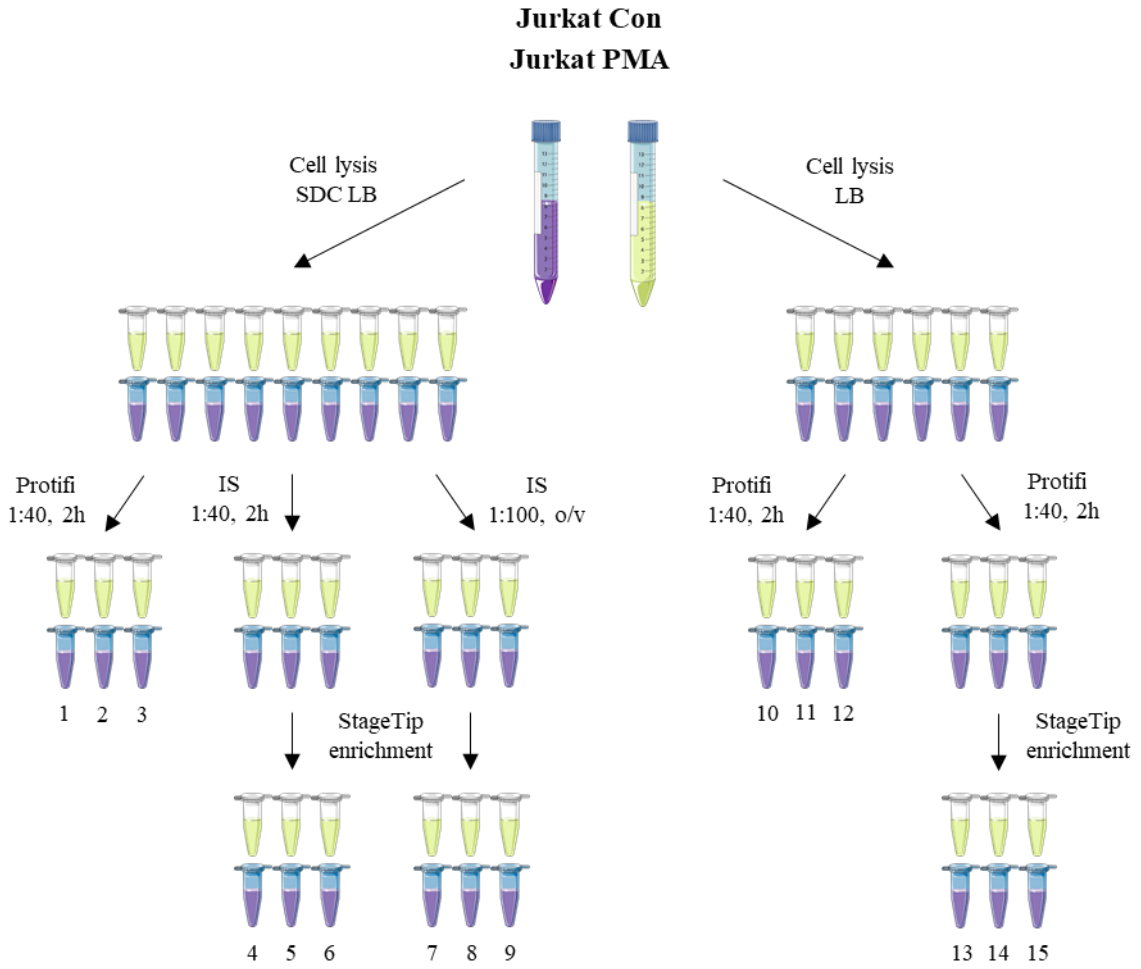

Figure 4 Experimental setup for the cell lysis, proteolytic digest and phosphopeptide enrichment steps. [1]

3.3.1. Protifi® S-trap™ micro/mini protein digestion

Samples for the analysis of the background proteome were diluted to a protein concentration of 1 µg/µL in 1.5 mL Eppendorf tubes. In detail, samples that were lysed with SDC lysis buffer (Jurkat Con 1-3, Jurkat PMA 1-3) were diluted to a total of 20 µg protein in 20 µL SDC lysis buffer with 5% (v/v) SDS to avoid precipitation. Samples that were lysed using hypotonic lysis buffer (Jurkat Con 10-12, Jurkat PMA 10-12) were diluted to a total of 20 µg protein in 20 µL Protifi® lysis buffer. Samples that should be subsequently phosphopeptide enriched were diluted to a protein concentration of 4 µg/µL in 1.5 mL Eppendorf tubes. In detail, samples that were lysed using hypotonic lysis buffer (Jurkat Con 13-15, Jurkat PMA 13-15) were diluted to a total of 200 µg protein in 50 µL Protifi® lysis buffer. Protein digestion was performed using Protifi® S-trap™ micro columns for background proteome samples and Protifi® S-trap™ mini columns for samples with subsequent phosphopeptide enrichment. 20/50 µL 64 mM DTT (for micro/mini columns) were added to each sample followed by incubation at 300 rpm, 95°C for 10 minutes on a thermoshaker (Eppendorf ThermoMixer®) for the reduction of disulfide bonds. The samples were cooled to room temperature and centrifuged at 1,000 x g for 1 minute. To alkylate cysteine residues, 5/12.5 µL 486 mM IAA were added, followed by incubation at 300 rpm, 30°C for 30 minutes in the dark on a thermoshaker. The samples were acidified by addition of 4.5/11.25 µL 12% (v/v) phosphoric acid. 297/866 µL S-Trap buffer (90% (v/v) MeOH, 100 mM TEAB) were added and 175/500 µL of the lysates were transferred to Protifi® S-trap™ micro/mini columns. The columns were placed in 2 mL Eppendorf tubes and centrifuged at 1,000 x g for 1 minute. The remaining lysates were transferred to the columns, columns were rotated by 180° and centrifugation was repeated. The columns were washed by adding 150/400 µL S-Trap buffer and centrifuging at 1,000 x g for 1 minute. The process was repeated three times and the columns were rotated by 180° between each wash step. Flow-throughs were discarded and the columns were transferred to new 2 mL Eppendorf tubes after the final wash step. 20 µg of Trypsin/Lys-C mix (Promega) were dissolved in 800/500 µL digestion buffer (50 mM TEAB) and stored on ice. 20 µL of Trypsin/Lys-C with c= 25 ng/µL (0.5 µg enzyme) were added to the Protifi® S-trap™ micro columns, 125 µL of Trypsin/Lys-C with c= 40ng/µl (5µg enzyme) were added to the Protifi® S-trap™ mini columns. Columns were capped and protein digestion was performed at 37°C for 2 hours in an incubator (Heratherm™ Compact Incubator, Thermo Scientific™). Peptides were eluted by addition of 40/80 µL digestion buffer directly onto the digestion solution and centrifugation at 1,000 x g for 1 minute. Peptide elution was continued by adding 40/80 µL 0.2% (v/v) FA, repeating centrifugation, adding 35/80 µL 50% (v/v) ACN, 0.2% (v/v) FA and completed by a final centrifugation step.

Samples were dried in a vacuum concentrator at 40°C and stored at -20°C until further processing.

3.3.2. In solution protein digestion

The samples Jurkat Con 4-9 and Jurkat PMA 4-9 were diluted to a total of 200 µg protein in 270 µL SDC lysis buffer. 30 µL reduction/alkylation buffer (100 mM TCEP, 400 mM 2-CAM, brought to pH 7-8 with 5M NaOH) were added to the samples followed by incubation at 1,400 rpm, 45°C for 5 minutes in the dark on a thermoshaker. The samples were cooled to room temperature. 20 µg of Trypsin/Lys-C mix (Promega) were dissolved in 20 µL trypsin buffer (0.05% (v/v) acetic acid, 2 mM $CaCl_2$) and kept on ice. Enzyme was added to the samples at an enzyme to substrate ratio of 1:100 (2 µL) followed by an overnight digest at 1,400 rpm and 37°C on a thermoshaker.

3.3.3. TiO_2 Phosphopeptide enrichment

For phosphopeptide enrichment, a slightly modified version of the EasyPhos workflow [19] was applied. Samples that were digested via Protifi® S-trap™ mini columns and dried were resuspended in 300 µL SDC lysis buffer. Samples that were digested via in solution digestion were further processed without any modification. 400 µL isopropanol were added to each sample and mixed at 1,400 rpm for 30 seconds on a thermoshaker. 100 µL EP enrichment buffer (48% (v/v) TFA, 8 mM KH_2PO_4) were added and mixed at 1,400 rpm for 30 seconds on a thermoshaker. Titansphere ®TiO beads (GL Sciences Inc.) were resuspended in EP loading buffer (6% (v/v) TFA, 80% (v/v) ACN) at a concentration of 1 mg/µL. An aliquot of 3 µL was pipetted into each sample and incubated at 1,400 rpm, 40°C for 5 minutes on a thermoshaker. The beads were pelleted by centrifugation at 2,000 x g for 1 minute and the nonphosphopeptide supernatant was discarded. 1 mL EP wash buffer (5% (v/v) TFA, 60% (v/v) isopropanol) was added, the beads were resuspended briefly by vortexing (Vortex-Genie® 2) and incubated at 1,400 rpm for 30 seconds on a thermoshaker. The beads were pelleted by centrifugation at 2,000 x g for 30 seconds and the supernatant was carefully discarded. The washing process was repeated four times. After the final wash step, the beads were resuspended in 75 µL EP transfer buffer (0.1% (v/v) TFA, 60% (v/v) iPrOH) and transferred to the top of a C_8-StageTip (CDS C8 Solid Empore™ Extraction Disks in pipette tips). Another 75 µL EP transfer buffer were added to the sample tubes to capture any remaining beads and transferred to the StageTips. The StageTips were placed in Eppendorf tubes for collecting the flow-through and centrifuged at 1,500 x g for 8 minutes. The flow-through was discarded and any remaining beads in the sample

tubes were captured by another 75 µL EP transfer buffer that were again added to the StageTips. Centrifugation was repeated, followed by placing the StageTips in new 1.5 mL Eppendorf tubes. Phosphopeptides were eluted by adding 30 µL EP elution buffer (40% (v/v) ACN, 25% (w/v) ammonium hydroxide) onto the StageTips and centrifuging at 1500 x g for 4 minutes. The process was repeated and the StageTips were rotated between centrifugation steps. The samples were finally dried in a vacuum concentrator (miVac Duo, Genevac™) at 40°C and stored at -20°C until further processing.

3.4. nanoLC-MS/MS analysis

3.4.1. Nano Liquid Chromatography

Phosphopeptide enriched samples were reconstituted in 15 µL MS loading buffer (97.7% (v/v) H_2O, 2% (v/v) ACN, 0.3% (v/v) TFA), centrifuged at 15,000 x g for 2 minutes and transferred to sample vials. Non-enriched samples were reconstituted in 5 µL 10 fmol/µl standardpeptide-mixture (in 30% (v/v) FA) and diluted with 40 µL eluent A (97.9% (v/v) H_2O, 2% (v/v) ACN, 0.1% (v/v) FA). 5-10 µL of sample were introduced into a Dionex 3000 nanoRSLC system, equipped with a C18 trapping column (2 cm x 100 µm, 3 µM particle size, C18, Thermo Fisher Scientific) and subsequent C18 analytical column (50 cm x 75 µm, 2.6 µM particle size, C18, Thermo Fisher Scientific). Subsequently, they were separated by elution from the pre-column to an analytical column applying a flow rate of 400 nL/min and using a gradient of 8% to 40% eluent B (80% ACN, 20% H2O, 0.1% FA) over 95 min, resulting in a total LC run time of 135 min including washing and equilibration steps.

3.4.2. Mass Spectrometer Parameters

Mass spectrometric analyses were accomplished using the timsTOF™ Pro mass spectrometer (Bruker Daltonics Inc.) coupled to a captive spray ion source run at 1600 V. Furthermore, the mass spectrometer was operated in the Parallel Accumulation-Serial Fragmentation (PASEF) mode. Trapped ion mobility separation was performed by applying a $1/K_0$ scan range from 0.60 – 1.60 Vs/cm^2 resulting in a ramp time of 166 ms. All experiments were performed with 10 PASEF MS/MS scans per cycle leading to a total cycle time of 1.88 s. MS and MS/MS spectra were recorded using a scan range (m/z) from 100 to 1700. Furthermore, the collision energy was ramped as a function of increasing ion mobility from 20 to 52 eV and the quadrupole isolation width was set to 2 Th for $m/z < 700$ and 3 Th for $m/z > 700$.

3.5. Data Processing

For the preliminary qualitative analysis of the obtained dataset, the software package PEAKS Studio X+ (version 10.5) [57] was used. For positive protein identification, at least one unique peptide had to be detected. In the digestion mode, Trypsin/P was specified. The Peptide mass tolerance was fixed to 15 ppm for MS1 level and fragment tolerance level to 0.05 Da. A value of 0.01 was set for the false discovery rate (FDR) on peptide and protein level. The human UniProt database (version 02/2020) [14] was applied for the search. As fixed modification, Carbamidomethylation was set. Phosphorylation of serine, threonine and tyrosine, N-terminal acetylation, methionine oxidation and deamidation of asparagine and glutamine were set as variable modifications. A maximum of two missed cleavages was allowed for each peptide. Each peptide was allowed to have a maximum of two missed cleavages.

For the evaluation of site specificity of phosphorylation events, the calculated A-score cut-off was set to 6.02 and 1.25 for class I and class II sites, respectively.

For the quantitative analysis of the dataset, a combined approach of the software tools MSFragger (version 2.3) [58] and Skyline [59] was employed. Peptide and protein identification results were obtained from MSFragger, set to the above mentioned parameters. Skyline was used as an integration tool to obtain reliable quantitative values for all identified peptides. Statistical analysis results of differentially abundant peptides and proteins were obtained from Skyline.

4. Results

Control and PMA- treated Jurkat samples from the prepared background proteome and phosphoproteome were analyzed via IMMS as described in section 3.4.

4.1. Technical parameters

For the initial evaluation of the dataset, technical parameters such as precursor distributions in all dimensions and correlations of measured ion mobility values were analyzed in PEAKS Studio.

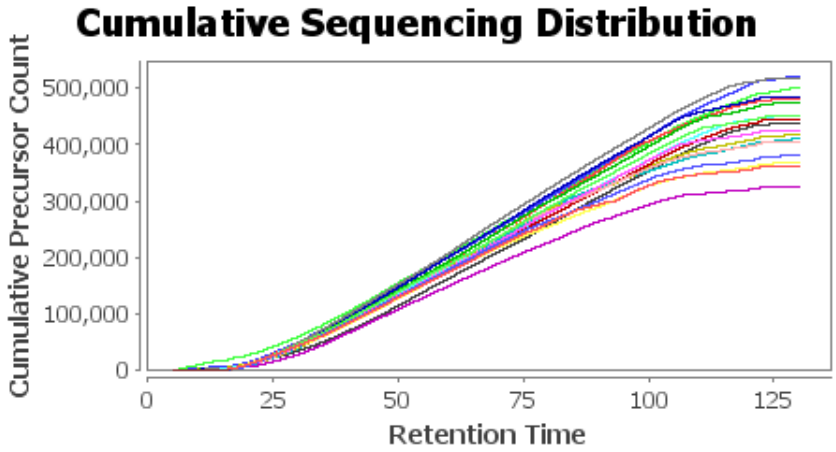

Figure 5 Cumulative sequencing distribution showing precursor count over retention time. Data includes all enriched samples.

As illustrated in Figure 5, the chromatographic performance can be evaluated by the cumulative precursor count over retention time, indicating a reproducible and efficient separation over the whole gradient.

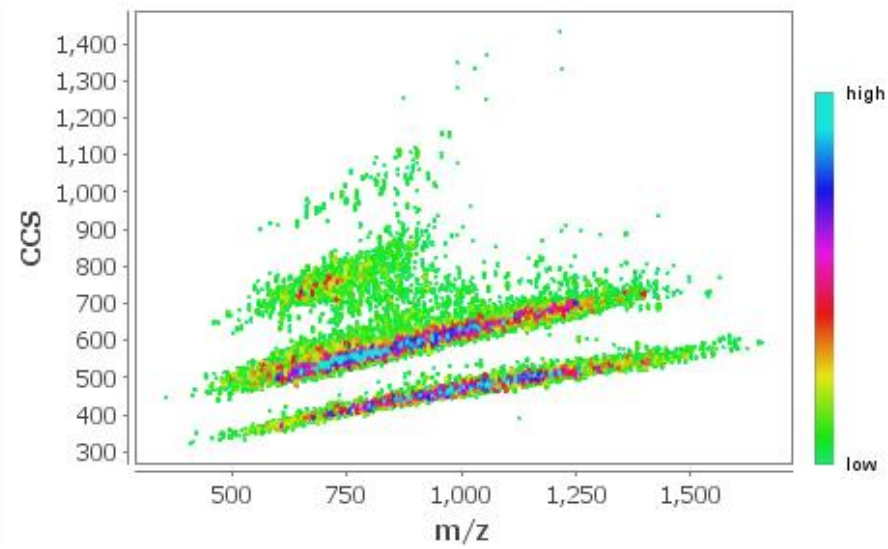

Figure 6 CCS plot of identified features over all enriched samples.

Figure 6 shows the distribution of identified features with respect to their ion mobility behavior, demonstrated by plotting m/z values against CCS values. A distinct pattern of multiple charged features with a clear separation between $[MH_2]^+$ - $[MH_4]^+$. In case of enriched samples, the dominant ion mobility "cloud" corresponds triple charged precursors.

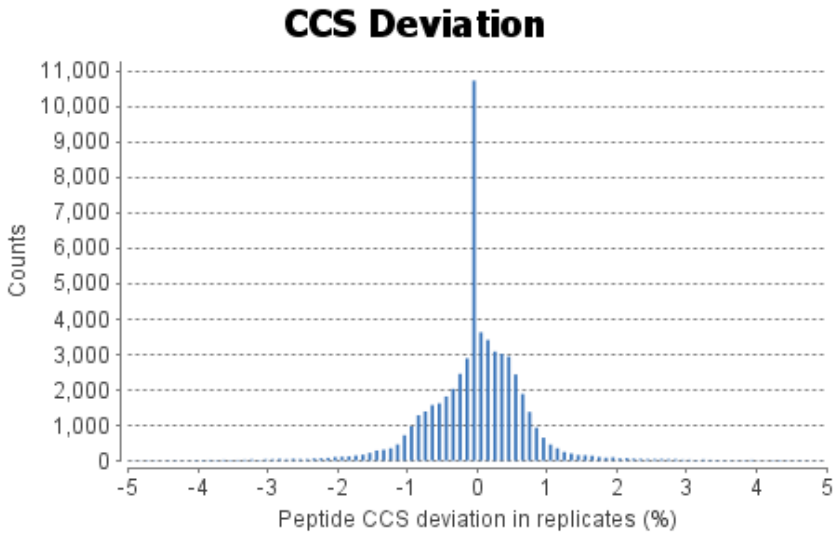

Figure 7 Distribution of peptide CCS deviation over all enriched samples.

In order to evaluate the robustness of measured CCS values, the percentage of deviation of matched peptides over all enriched samples was plotted in Figure 7, demonstrating an overall reliable and robust assignment of CCS values with almost all matched peptides within a one percent margin.

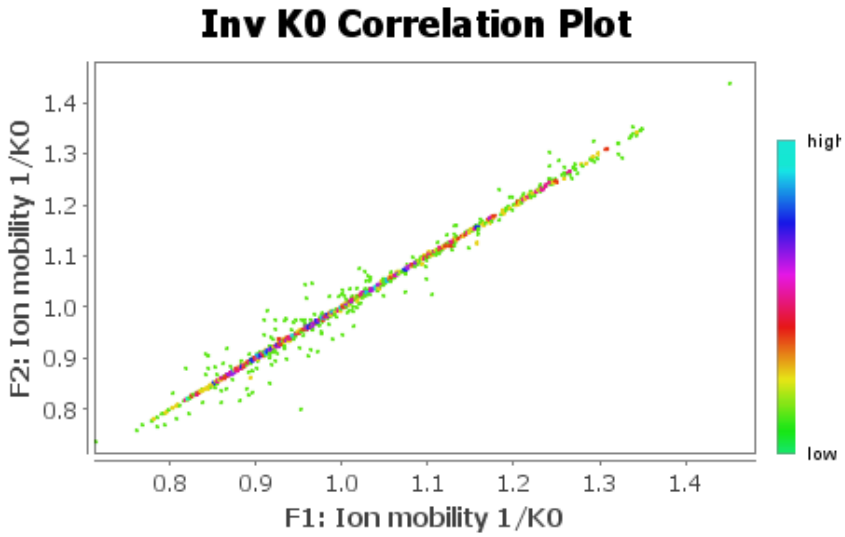

Figure 8 Correlation plot of inverse K_0 ion mobility values between two biological replicates of the enriched control cohort.

Similar to Figure 7, Figure 8 illustrates the correlation of inverse K_0 values of identified precursors between two biological replicates of the control cohort, showing high correlation of almost all precursors with only some deviation for low abundant precursors.

4.2. Evaluation of protein digestion methods for phosphopeptide enrichment

In order to evaluate which protein digestion method in combination with subsequent phosphopeptide enrichment yields the highest number of identified peptides and phosphopeptides, different digestion protocols were evaluated. The evaluation was based on the numbers of identified peptides and performed in PEAKS Studio. A filter-assisted digest using Protifi® S-trap™ columns was performed with an enzyme to substrate ratio of 1:40 and a digestion time of 2 h. An in-solution digest was performed at the same conditions, as well as with an enzyme to substrate ration of 1:100 digested overnight. Each digest condition was performed in triplicate. First, the number of identified peptides and the overlaps between the methods were compared by considering all peptides that were identified in at least one triplicate of the corresponding conditions and exhibited a precursor intensity of at least 250. In the control samples, the overnight in-solution digest in combination with subsequent phosphopeptide enrichment yielded in the highest number of identified peptides (6,913), followed by the in-solution digest for 2 h (5,746) and the Protifi®- digest (3,891) (Figure 9). In the PMA-treated samples, similar results were observed, the highest number of peptides was identified in the in-solution overnight-digested samples as well (6,996), followed by the in-solution digest for 2 h (5,493) and the Protifi®-digest (4,752).

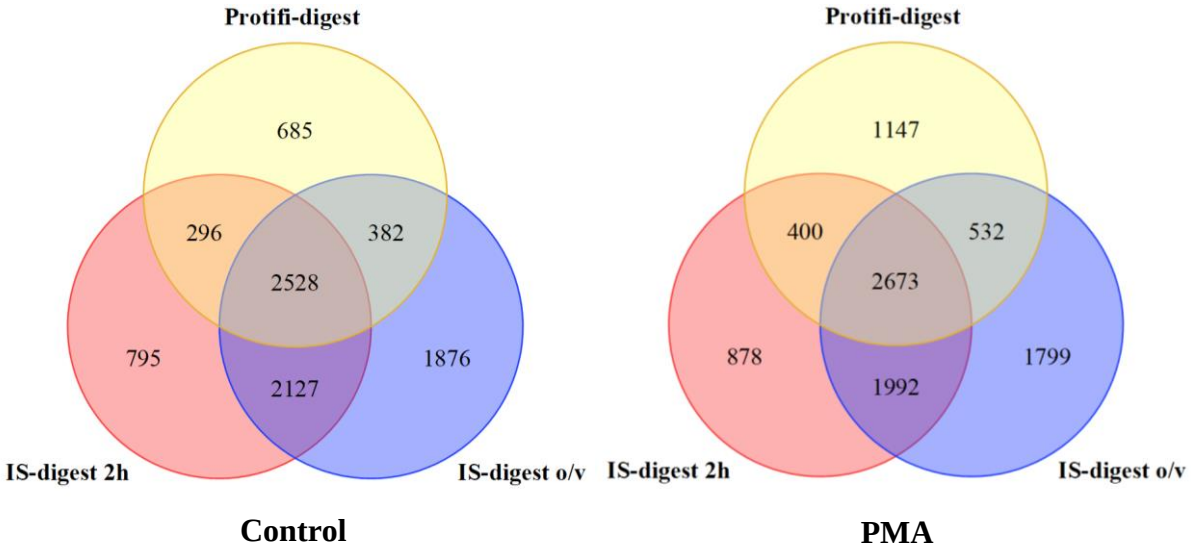

Figure 9 Number of identified peptides and overlaps between the evaluated digestion methods in control and PMA treated samples with each peptide being identified in at least one triplicate of the corresponding condition. Protifi® digest was performed at 2 h with an enzyme to substrate ration of 1:40, in-solution digest was performed for 2 h with an enzyme to substrate ratio of 1:40 and overnight with an enzyme to substrate ratio of 1:100.

Similar results were obtained when considering only peptides that were identified in each replicate of the corresponding conditions (Figure 10).

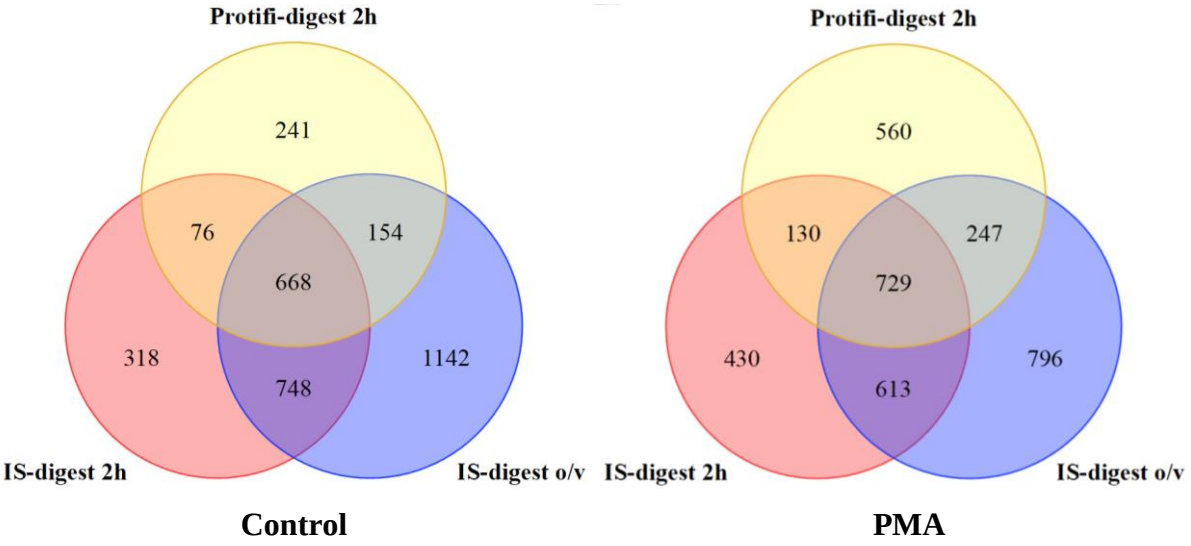

Figure 10 Number of identified peptides and overlaps between the evaluated digestion methods in control and PMA treated samples with each peptide being identified in each triplicate of the corresponding condition.

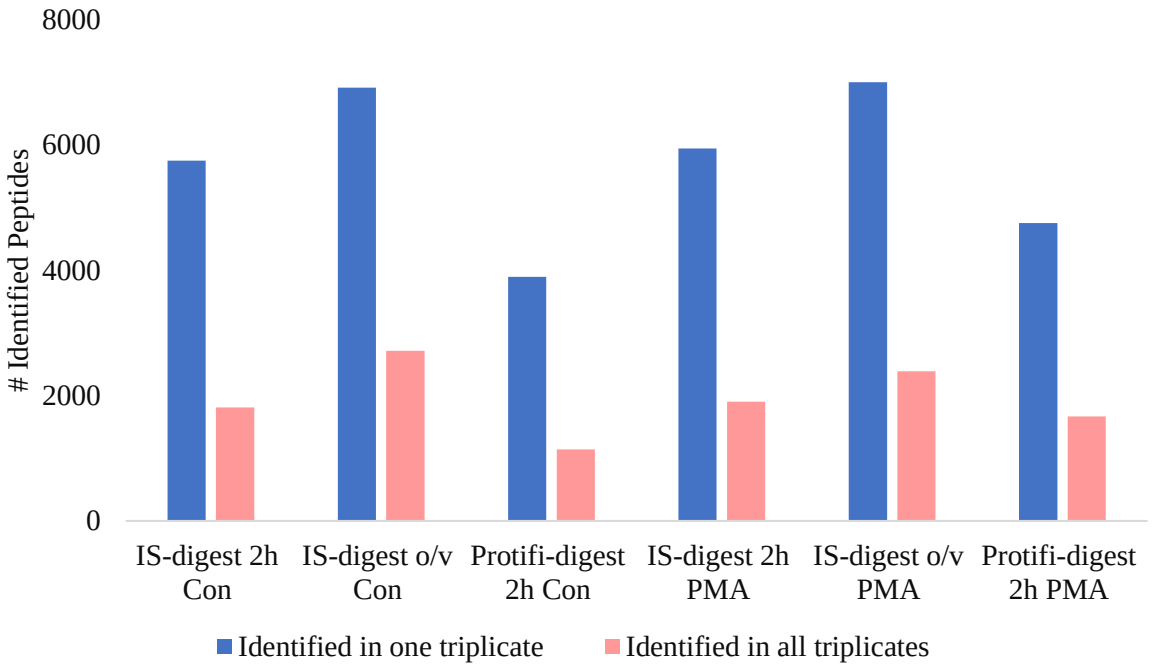

Figure 11 Comparison of peptides identified in one vs. in all triplicates.

When comparing the ratio between peptides identified in only one replicate of each condition and peptides identified in each triplicate, the in-solution overnight digest yielded the best ratio in control samples (39%), whereas in the PMA-treated samples it was slightly outperformed by the Protifi-digest (35% vs. 34%). In total, the in-solution overnight digest with an enzyme to substrate ratio of 1:100 outperformed the other digestion methods in the number of identified peptides in control and PMA-treated samples when considering the peptides identified in one triplicate, but also for all triplicates. (Figure 11)

4.3. Phosphopeptide enrichment efficiency

As the goal of phosphopeptide enrichment is to maximize the number of identified phosphopeptides and minimize the number of non-phosphorylated peptides, the percentage of identified phosphopeptides is a suitable indicator for the success of a phosphopeptide enrichment. In the phosphopeptide enriched samples, grouped together and entitled as the phosphoproteome, a total number of 11,393 peptides were identified, containing 11,110 phosphopeptides, which equals an enrichment factor of 98% (Figure 12). In the samples of the background proteome, which were not undertaken phosphopeptide enrichment, a total number of 44,718 peptides was identified, containing only 894 phosphopeptides, accounting for only 2% of the total peptide number. When comparing the number of identified phosphopeptides in the background proteome and the phosphoproteome, a fold increase of 12.42 was achieved by the phosphopeptide enrichment.

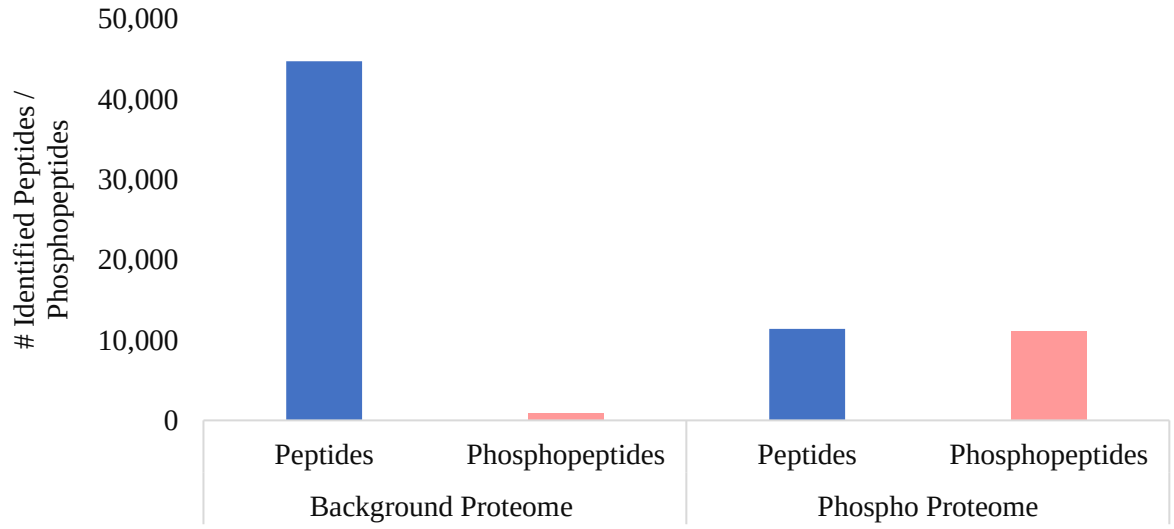

Figure 12 Comparison of the numbers of identified peptides and phosphopeptides in the Background and the Phospho Proteome. In the background proteome, only 2% of the identified peptides were phosphopeptides, whereas in the phospho proteome, phosphopeptides accounted for 98% of identified peptides.

4.4. Phosphopeptide class distribution

In order to assess the site confidence of the identified phosphosites, the phosphopeptides identified in the phosphoproteome were classified according to their Ascore. The classification was performed in PEAKS Studio.

The Ascore is a probability-based score for the correct phosphosite localization that uses exclusively site-determining fragment ions of an MS/MS spectrum for its calculation. [29] The Ascore cut-off values and corresponding phosphosite localization probabilities used for classification can be found in Table 1.

In the phosphoproteome, 70% peptides of all identified phosphopeptides were classified as class I peptides, 6% as class II peptides and 24% as class III peptides. The phosphopeptide class distribution can be found in Figure 13.

Table 1 Ascore cut-offs and corresponding phosphosite localization probabilities for the annotation of phosphopeptide class I, II and III.

Phosphopeptide class	Ascore	Phosphosite localization probability
I	> 6.02	> 75%
II	> 1.25	25-75%
III	< 1.25	< 25%

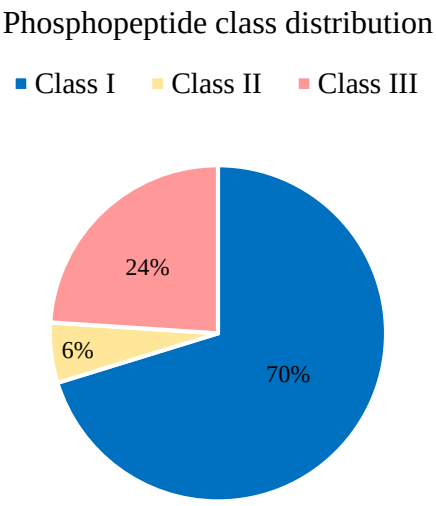

Figure 13 Phosphopeptide class distribution in the phosphoproteome. The majority of the identified phosphopeptides was classified as class I, exhibiting a phosphosite localization probability of over 75%. Only 6% were classified as class II and 24% as class III. The Ascore cut-off values and corresponding phosphosite localization probabilities can be found in Table 1.

4.5. Reproducibility of biological replicates

After performing the statistical evaluation of phosphopeptide enrichment strategies and the analysis of phosphopeptide class distribution in PEAKS studio, the further in detail technical and biological interpretation as well as quantitative analysis was performed only with the results from samples digested overnight via in-solution digest, as this method yielded the best results. For further analysis, data was processed via MSFragger and Skyline.

In the background proteome, 4,478 proteins and 40,625 peptides, including 769 phosphopeptides, were identified. In the phosphoproteome, 1,375 proteins and 10,172 peptides, including 10,075 phosphopeptides, were identified.

When comparing the peak area CVs among the triplicates of the background proteome and the phosphoproteome of both conditions, PMA-treated samples exhibited lower median CVs (24.0% background proteome, 25.4% phosphoproteome, Figure 15Figure **17**) than the control samples (32.6% background proteome, 48.3% phosphoproteome, Figure 14Figure **16**).

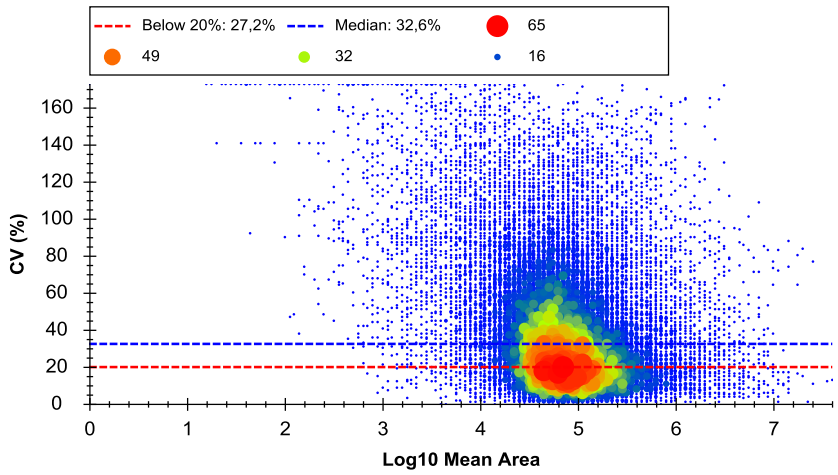

Figure 14 Peak Areas CV Histogram of control samples in the background proteome. (Not normalized)

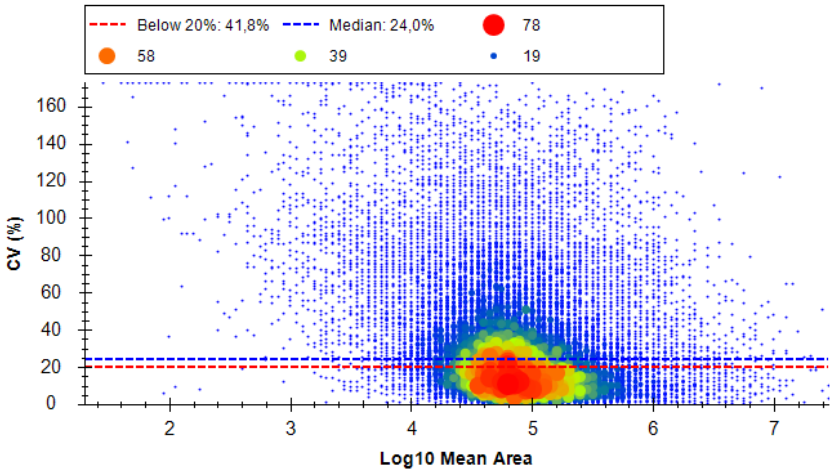

Figure 15 Peaks Areas CV Histogram of PMA-treated samples in the background proteome. (Not normalized)

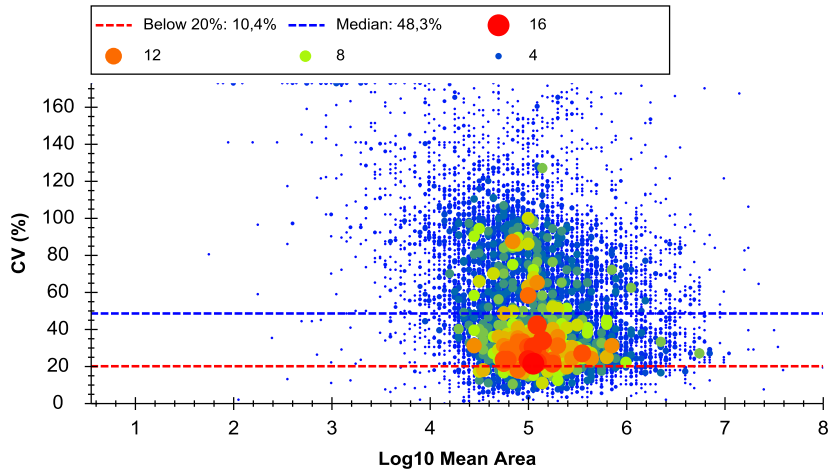

Figure 16 Peak Areas CV Histogram of control samples in the phosphoproteome. (Not normalized)

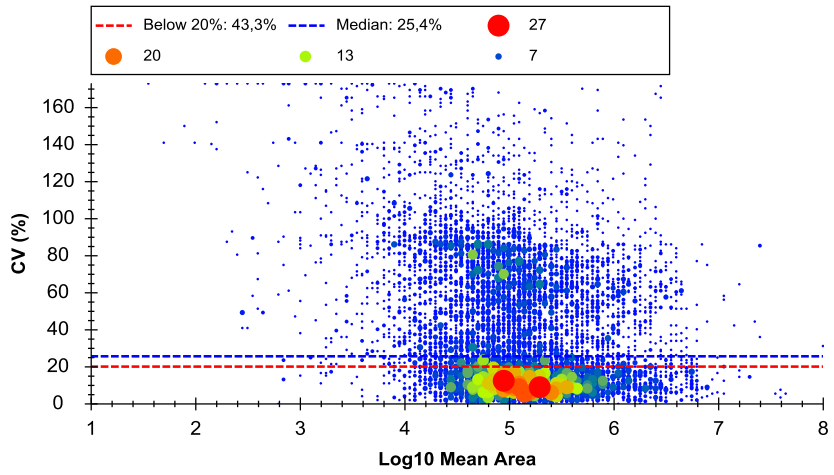

Figure 17 Peak Areas CV Histogram of PMA-treated samples in the phosphoproteome. (Not normalized)

4.6. Protein regulations – Background Proteome

In the background proteome, out of 4,478 identified proteins, only four proteins were found to be significantly upregulated (fold change cutoff of 2, adjusted p-value cutoff of 0.05) upon PMA treatment and no downregulations were observed (Figure 18).

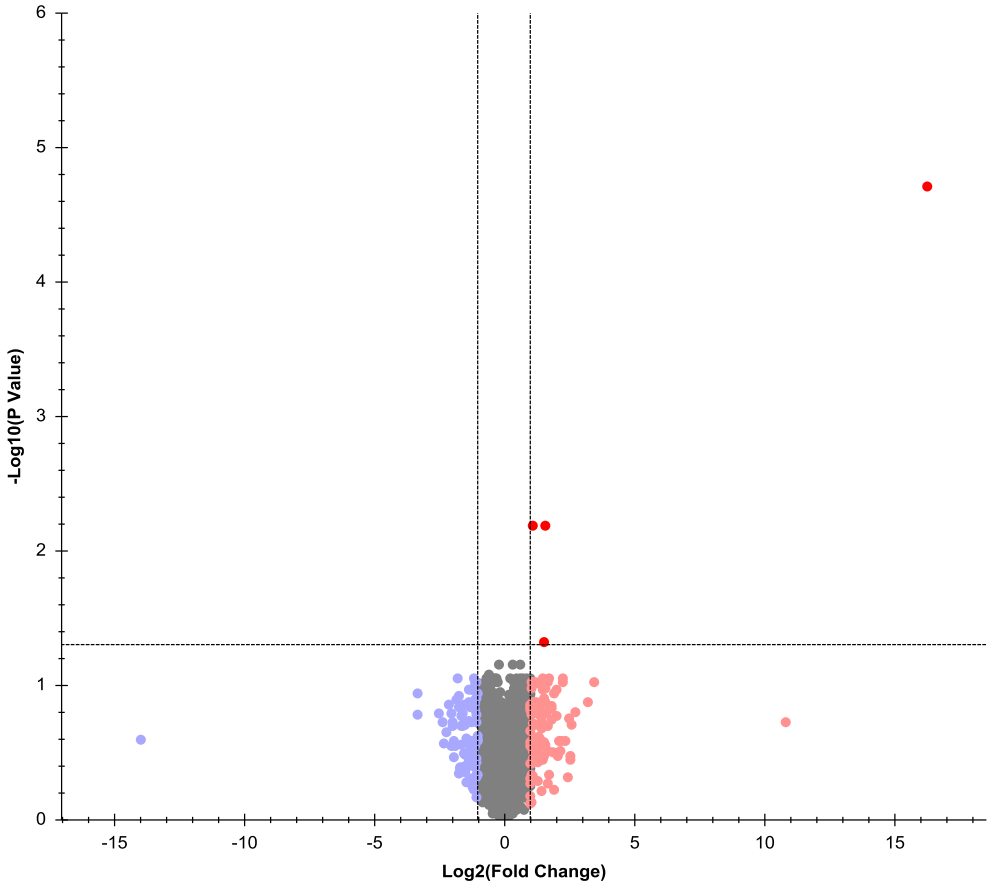

Figure 18 Volcano Plot of proteins identified in the background proteome.

The proteins that were found to be upregulated are the early growth response protein 1 (EGR1), the prenylated rab acceptor protein 1 (PRAF1), the mitochondrial NADH dehydrogenase protein 4 (NDUS4) and the dedicator of cytokinesis protein 11 (DOC11). A list of the upregulated proteins including their log 2 fold changes and the adjusted p-values can be found in Table 2. EGR 1 is a regulator of transcription for different target genes. PRAF 1 is a regulator of the Rab protein and is required for the vesicle formation from the Golgi apparatus. NDUS 4 is a subunit of the mitochondrial membrane respiratory chain NADH dehydrogenase. DOC 11 is a guanine-exchange factor, activates CDC42 and plays a role in B-cell development. [14]

Table 2 Regulated proteins in the background proteome.

Protein Name	UniProt ID	UniProt Entry Name	Log 2 Fold Change	Adjusted P-value
Early growth respone protein 1	P18146	EGR1_HUMAN	16.2902	0.0000
Prenylated Rab acceptor protein 1	Q9UI14	PRAF1_HUMAN	1.5982	0.0063
NADH dehydrogenase iron-sulfur protein 4, mitochondrial	O43181	NDUS4_HUMAN	1.5263	0.0484
Dedicator of cytokinesis protein 11	Q5JSL3	DOC11_HUMAN	1.0869	0.0063

4.7. Protein/Peptide regulations – Phosphoproteome

In the phosphoproteome, out of 1,375 identified proteins, twelve were found to be significantly upregulated (fold change cutoff of 2, adjusted p-value cutoff of 0.05) upon PMA treatment and seven proteins were significantly downregulated (Figure 9). A list of the regulated proteins can be found in Table 3. No overlap between the proteins regulated in the background proteome and the proteins regulated in the phosphoproteome was observed.

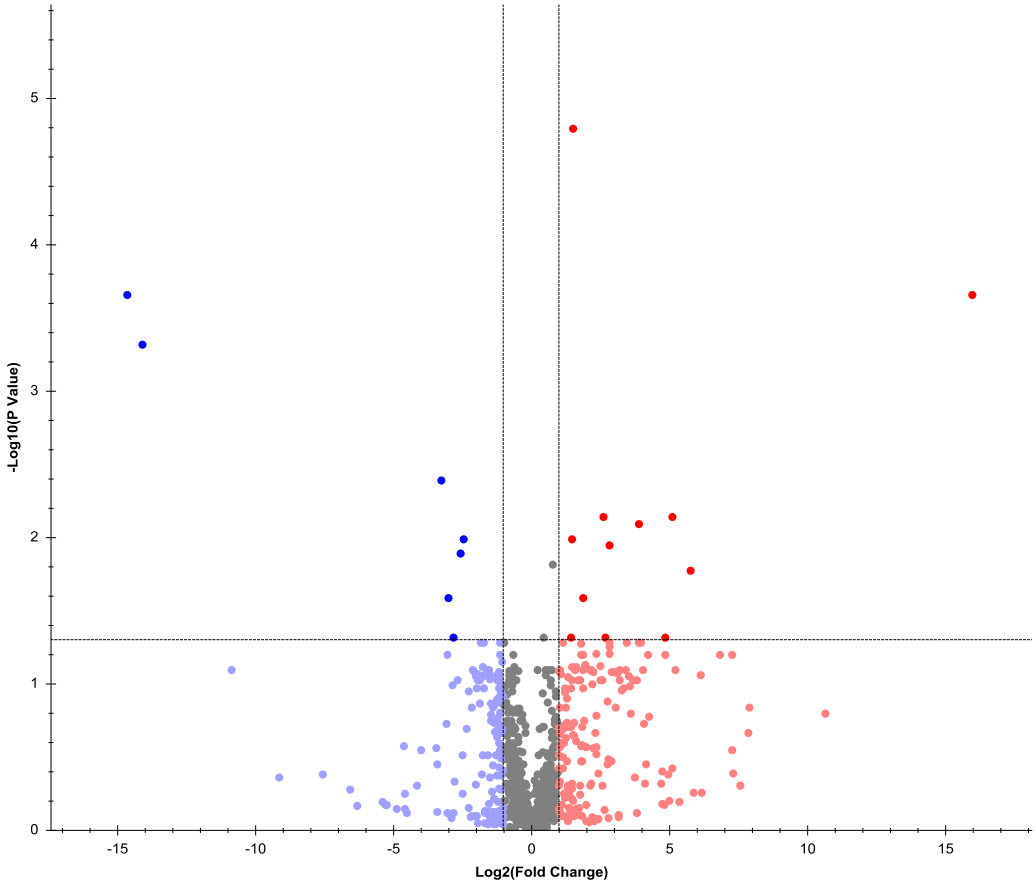

Figure 19 Volcano plot of proteins identified in the phosphoproteome.

Table 3 List of regulated proteins in the phosphoproteome: Cut-offs were set at 0.05 for adjusted p-value and log 2 fold change cut-off of 2.

Protein Name	UniProt ID	UniProt Entry Name	Log 2 Fold Change	Adjusted P-value
Protein kinase C delta type	Q05655	KPCD_HUMAN	15.9884	0.0002
T-cell surface glycoprotein CD3 gamma chain	P09693	CD3G_HUMAN	5.7735	0.0170
Vesicle-trafficking protein SEC22b	O75396	SC22B_HUMAN	5.1250	0.0073
NGFI-A-binding protein 2	Q15742	NAB2_HUMAN	4.8643	0.0483
Nuclear cap-binding protein subunit 1	Q09161	NCBP1_HUMAN	3.9116	0.0081
Neurobeachin-like protein 2	Q6ZNJ1	NBEL2_HUMAN	2.8272	0.0113
Src substrate cortactin	Q14247	SRC8_HUMAN	2.6220	0.0073
Protein Niban 2	Q96TA1	NIBA2_HUMAN	1.8863	0.0261
Condensin complex subunit 1	Q15021	CND1_HUMAN	1.4602	0.0483
Thymidine kinase, cytosolic	P04183	KITH_HUMAN	-2.5638	0.0130
Phospholipid transfer protein C2CD2L	O14523	C2C2L_HUMAN	-2.8243	0.0483
Arf-GAP domain and FG repeat-containing protein 1	P52594	AGFG1_HUMAN	-3.0114	0.0261
RAS protein activator like-3	Q86YV0	RASL3_HUMAN	-3.2511	0.0041
V-type immunoglobulin domain-containing suppressor of T-cell activation	Q9H7M	VISTA_HUMAN	1.5016	0.0103
Kinesin-like protein KIF15	Q9NS87	KIF15_HUMAN	2.6863	0.0483
Signaling threshold-regulating transmembrane adapter 1	Q9Y3P8	SIT1_HUMAN	1.5358	0.0000
Myc proto-oncogene protein	P01106	MYC_HUMAN	-2.4322	0.0103
Rab GTPase-activating protein 1-like	Q5R372	RBG1L_HUMAN	-14.6183	0.0002
Dysbindin domain-containing protein 2	Q9BQY9	DBND2_HUMAN	-14.0964	0.0005

On peptide level, 33 peptides were significantly downregulated and 60 peptides were significantly upregulated (Figure 20). A list of the regulated peptides can be found in Table 4 in the supplementary information. Biological and functional interpretation of the regulated peptides and proteins was supported by STRING analysis and can be found in chapter 4.7.1.

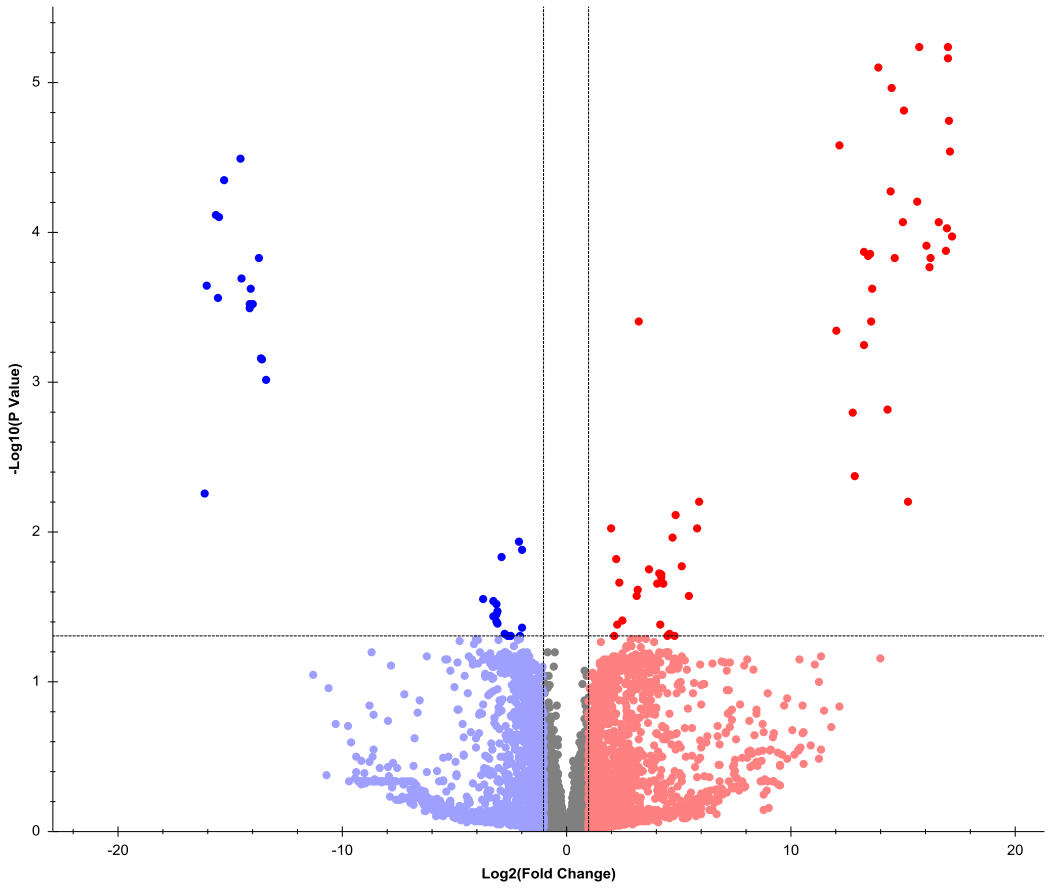

Figure 20 Volcano plot of peptides identified in the phosphoproteome.

PhosphoSitePlus [17], the largest phosphoproteomic MS-database, was used for the evaluation of the annotation of the phosphosites of the regulated peptides. Phosphosites were grouped into sites annotated with a biological function (upstream or downstream), annotated sites without biological function and not annotated sites. 49% of phosphosites of the regulated peptides were annotated with a biological function, 36% were annotated but not associated with a biological function and 15% were not annotated (Figure 21).

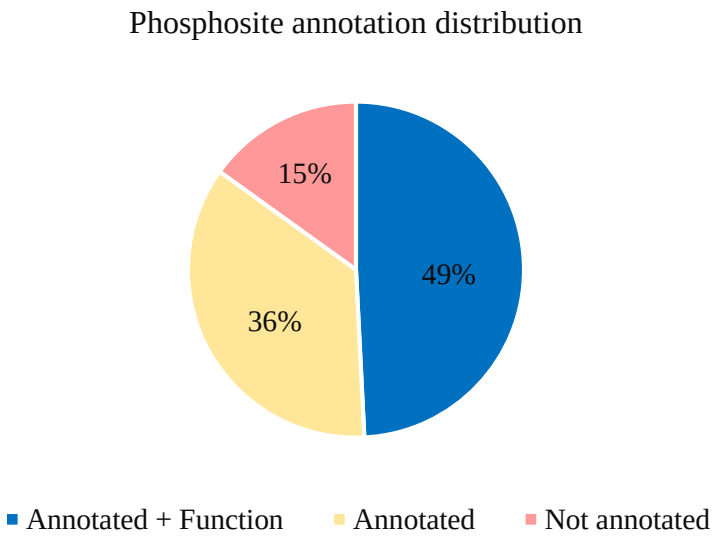

Figure 21 Distribution of phosphosite annotation classes among the regulated phosphopeptides in the phosphoproteome. Phosphosite annotation classes were defined as “annotated + function”, “annotated” and “not annotated”. Classification was based on the annotation of phosphosites in PhosphoSitePlus [17].

4.7.1. STRING analysis

The interpretation of proteome perturbation studies, especially on a biological and functional level, can be challenging. Therefore, protein interaction network analysis and gene ontology annotation with subsequent gene set enrichment analysis can be helpful tools for an unbiased and thorough functional interpretation on proteome scale.

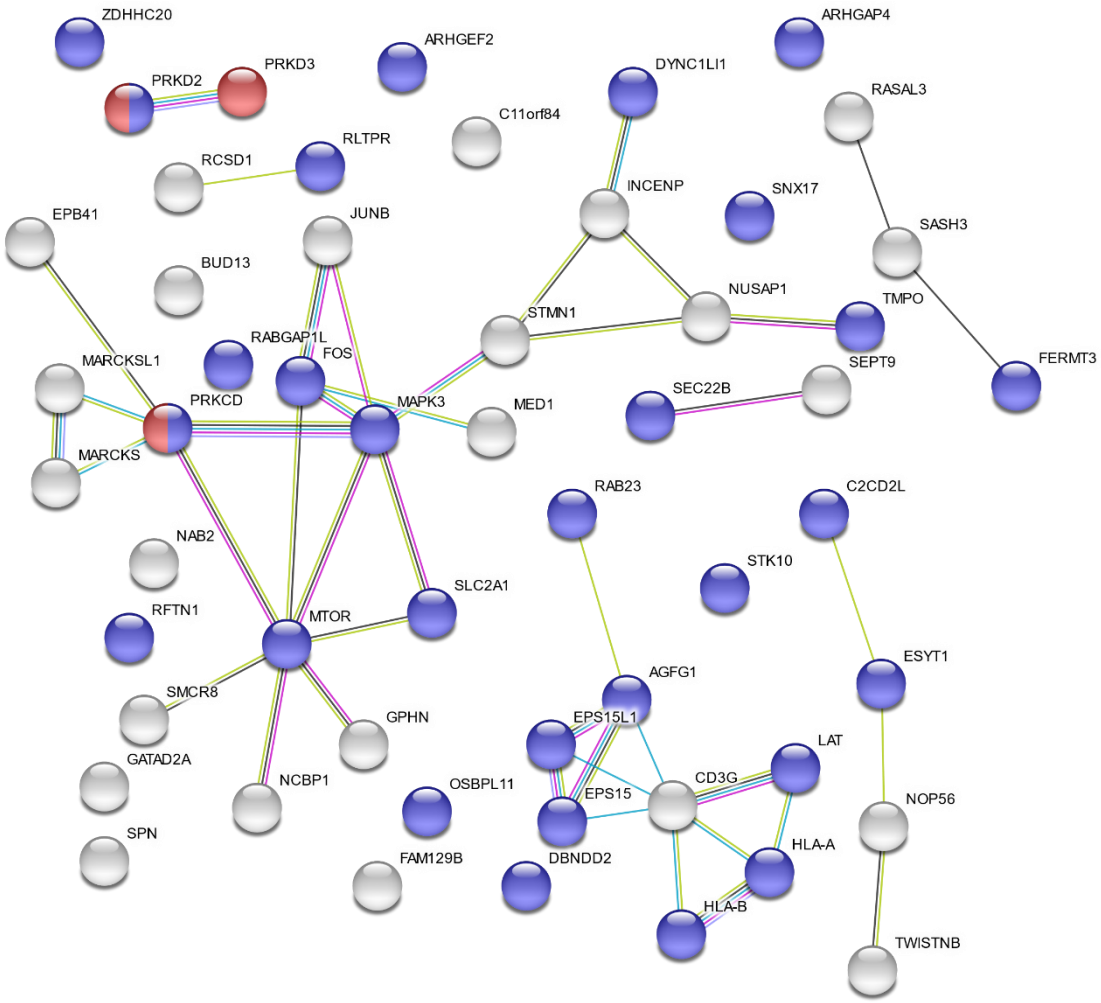

Figure 22 STRING analysis of proteins with regulated phosphorylated peptides. Links between protein nodes indicate a curated association. Red colored protein nodes annotate proteins with known phorbol ester binding sites. Blue colored nodes refer to endomembrane associated proteins [60].

The STRING analysis [60] of proteins with regulated phosphorylated peptides in the phosphoproteome, as shown in Figure 22, has yielded a rich protein interaction network describing regulated biological processes. Two main clusters can be seen, with central nodes CD3G and PRKCD/MAPK3, describing the main driving factors in this perturbation study. Additionally, a gene set enrichment analysis revealed significantly enriched clusters with implications on phorbol ester binding capability (p-value= 0.0027) and endomembrane system functionality (p-value= $3.47e^{-05}$).

4.8. Impact of Ion mobility on phosphoproteomic analysis

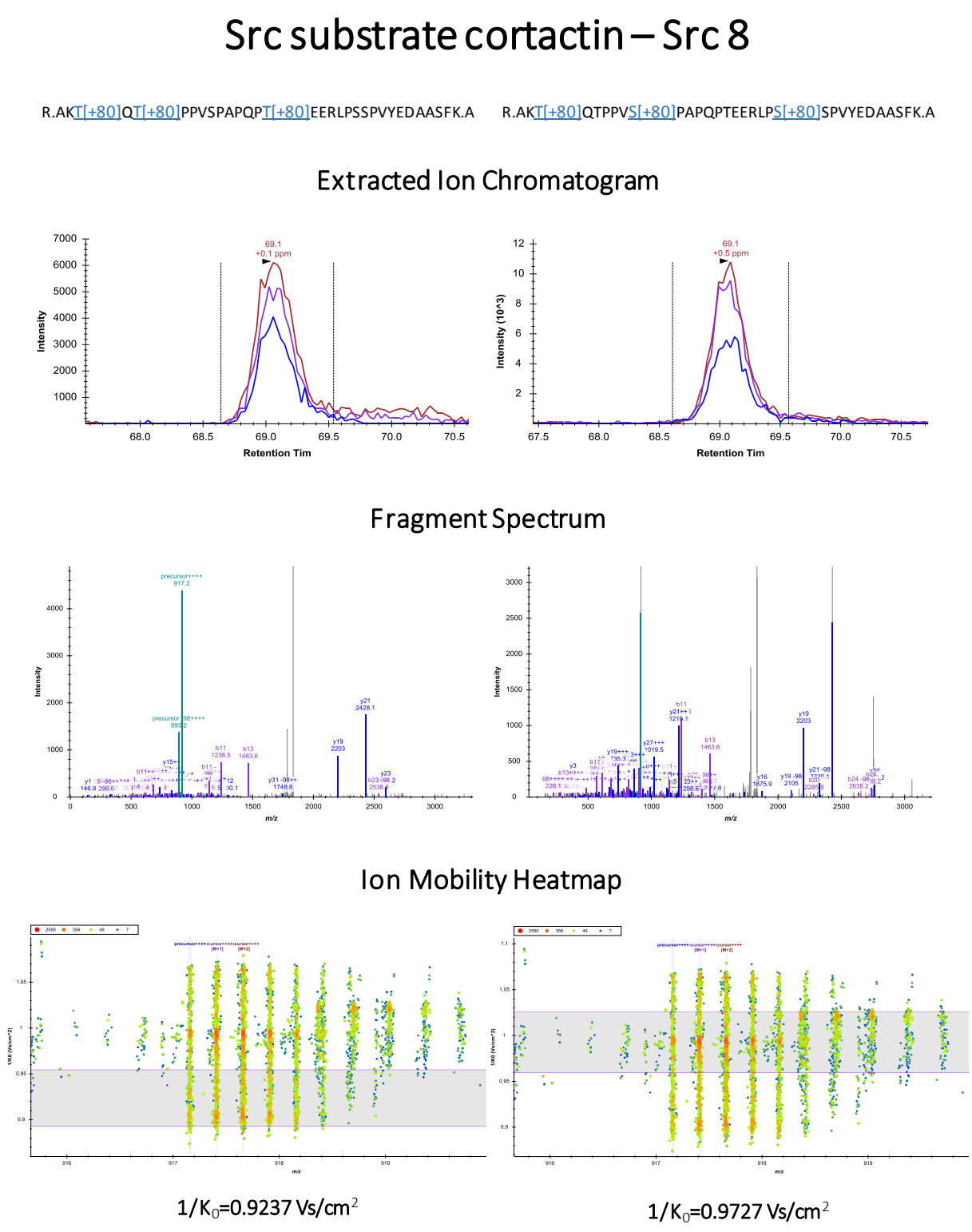

Figure 23 Extracted ion chromatograms, fragment spectra and ion mobility heatmaps of two different phospho-isoforms of the same peptide. The different phosphosites result in distinguishable CCS values, allowing for a separation by ion mobility.

As illustrated in Figure 23, different phospho-isoforms of the same peptide can exhibit different CCS values, resulting in distinguishable $1/K_0$ values. The peptides with the sequences AKT[+80]QT[+80]PPVSPAPQPT[+80]EERLPSSPVYEDAASFK and AKT[+80]QTPPV-S[+80]PAPQPTEERLPS[+80]SPVYEDAASFK exhibit $1/K_0$ values of 0.9237 Vs/cm^2 and 0.9727 Vs/cm^2, enabling their separation by ion mobility.

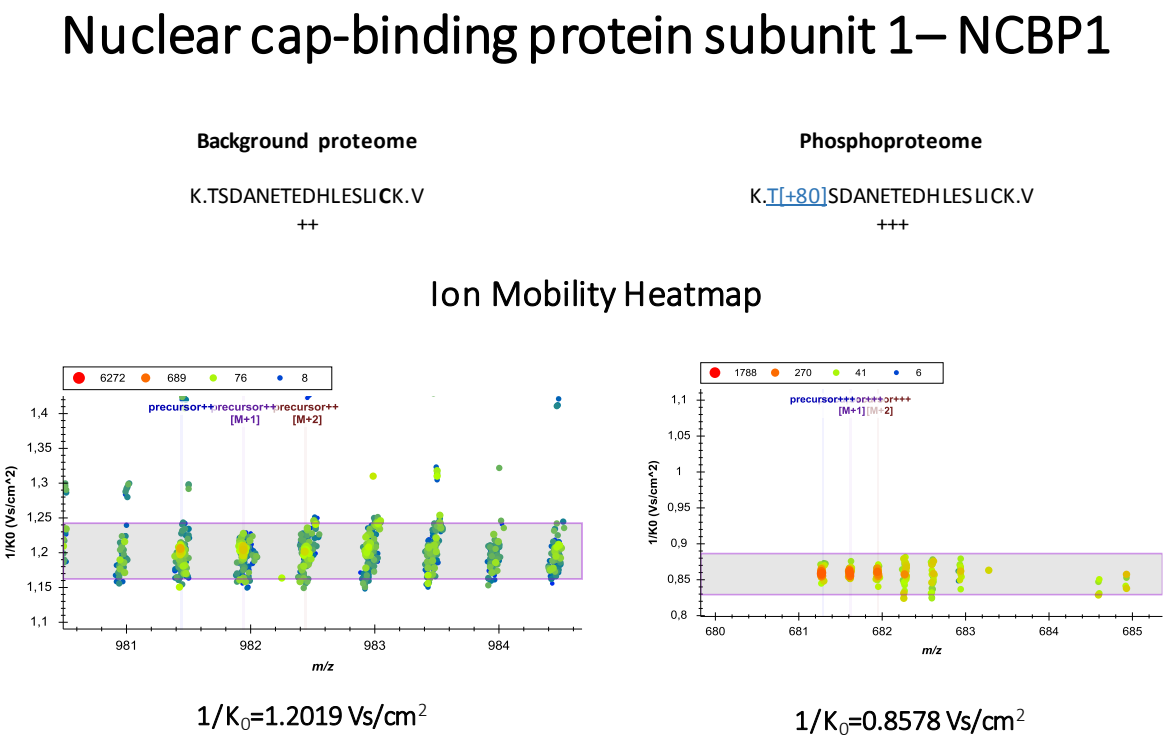

Figure 24 Ion mobility heatmap comparison of a phosphorylated peptide and its non-phosphorylated peptidoform.

As illustrated in Figure 24, the phosphorylation status of a peptide can influence the precursor charge state, which subsequently exerts a prominent effect on the retention during ion mobility separation, resulting in a different CCS value.

4.9. Jurkat cell imaging

As the phosphoproteomic results indicated major disturbances at the endomembrane system, fluorescence imaging can help to elucidate the morphological changes of said mechanism in a complementary fashion. As Figure 25 illustrates, already after 30 minutes of incubation with PMA at 10 ng/mL, strong changes in the morphology of the endoplasmatic reticulum (color gradient from blue to red) can be observed. In general, the focused areas seen in the control cohort seem to dissipate when PMA is applied. The cell membrane morphology shows no apparent alterations. When looking at the merged images, the clear distinction of nucleus and cytoplasm, as observed in the control cohort, becomes more diffuse after treatment.

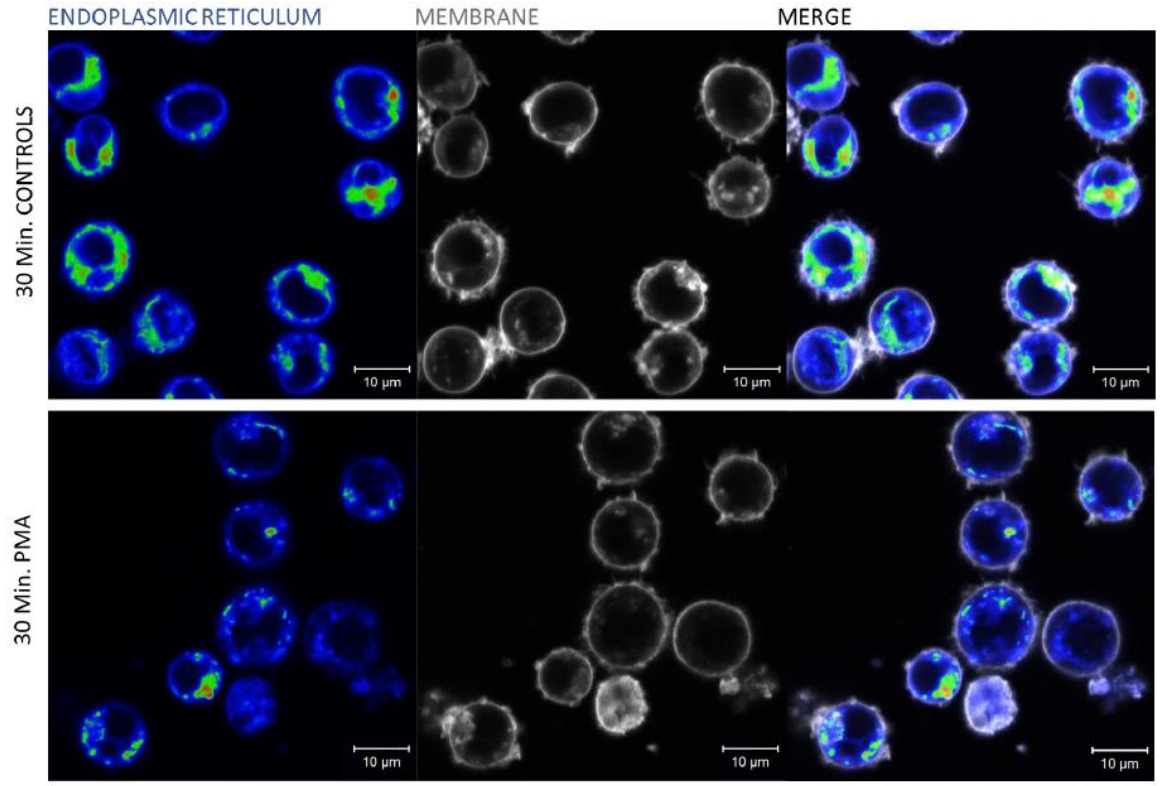

Figure 25 Fluorescence imaging of Jurkat cells after 30 min PMA stimulation. ER stain, membrane stain, merged image from left to right. Time matched controls on top, 30 min PMA stimulation at the bottom.

5. Discussion

When comparing the different protein digestion protocols for subsequent phosphopeptide enrichment via MOAC, the in-solution overnight digest with an enzyme to substrate ratio of 1:100 yielded the most peptide identifications overall. This was observed when considering peptides that were identified only in one triplicate, but also when considering only peptides that were identified in all triplicates. This is valid for control samples and PMA-treated samples equally. Therefore, this protein digestion method is the method of choice prior to phosphopeptide enrichment.

The high phosphopeptide enrichment factor of 98% obtained in the phosphoproteome is an indicator for successful phosphopeptide enrichment. In comparison, the low percentage of identified phosphopeptides in the background proteome further confirms the success of the applied phosphopeptide enrichment strategy and highlights the need for specific phosphopeptide enrichment techniques in order to facilitate the identification and further analysis of a high number of phosphopeptides.

The majority (70%) of the phosphopeptides identified in the phosphoproteome were classified as class I phosphopeptides, exhibiting a phosphosite localization probability of at least 75%. The highly confident phosphosite localization plays a major role in phosphoproteomics, as the distinction of phospho-peptidoforms is crucial for understanding phosphorylation events happening upon chemical pertubations or induced biological processes, enabling the identification of regulatory phosphosites.

While phospho-peptidoforms might be distinguished by different fragment spectra, the employment of ion mobility separation in phosphoproteomic MS analysis provides an additional dimension for separation of isoforms and can be seen as a powerful tool for phosphoproteomics. Although phospho-peptidoforms that differ in phosphosites in close proximity positioned in the center of the peptide might not show great difference in their CCS values, phosphopeptides differing in the position of many phosphosites or exhibiting distinct phosphosites at the peptide termini show different ion mobilities and can be distinguished via ion mobility separation. The technical parameters of the ion mobility measurements were evaluated as well and showed an overall robust and reliable assignment of the CCS values with nearly all matched peptides over the enriched samples, and a high correlation of $1/K_0$ values between biological replicates of the control samples, confirming the reliability of the performed ion mobility measurements.

Taken together, the combination of the optimal protein digestion method with subsequent phosphopeptide enrichment and sample analysis employing ion mobility mass spectrometry facilitated the identification of a large number of phosphopeptides, enabling a further functional analysis of the performed *in vitro* perturbation study based on the obtained phosphoproteome.

When comparing the control samples and the PMA treated samples both of the background proteome and the phosphoproteome, the PMA treated samples exhibited lower median CVs than the control samples. This might be explained by the fact that PMA was used as a chemical trigger on the *in vitro* cell system, inducing disturbances in the endomembrane system, leading to different matrix effects in comparison to the control samples and therefore resulting in lower CVs.

In the background proteome, only four proteins were found to be significantly upregulated upon PMA treatment. In contrast, twelve proteins were significantly upregulated and seven were significantly downregulated in the phosphoproteome, corresponding to 60 phosphopeptides and 33 phosphopeptides, respectively. The general observations confirm the hypothesis that after 3 hours of PMA treatment, protein expression in the background proteome is scarcely altered but signaling events can already be observed in a statistical significant manner.

The proteins corresponding to the regulated phosphopeptides of the phosphoproteome were undertaken a STRING analysis, resulting in clusters with CD3G and PRKCD/MAPK3. Furthermore, significantly enriched clusters revealed implications on phorbol ester binding capability confirming the successful treatment of the *in vitro* Jurkat cell system with PMA. The identified phosphosite pS299 of the protein PRKCD was indicated by Durgan et al. [55] to be a representative marker for the activation of the enzyme as it was demonstrated to be phosphorylated in mammalian cells upon phorbol ester stimulation. The regulated proteins and peptides in the phosphoproteome indicated disturbances in the endomembrane system. This finding was strongly supported by the fluorescence images taken, which showed major changes in the morphology of the endoplasmatic reticulum as well as a diffusion of the clear distinction of the nucleus and the cytoplasm.

The phosphosites of the regulated peptides in the phosphoproteome were classified according to their annotation in PhosphoSitePlus. Half of the phosphosites are annotated with a biological function, but 36% of the phosphosites are not annotated with a biological function and 15% are not annotated at all in PhosphoSitePlus. This underlines the fact that a large part of the phosphoproteome is still unexplored. Even if phosphosites are confidently identified in

proteomic/phosphoproteomic experiments, their functional annotation, including identification of their kinases, is complex and challenging.

Without phosphoproteomic analysis additional to a normal proteomic analysis, significant phosphoproteomic changes confirming the successful PMA treatment of the *in vitro* Jurkat cell model would have been missed out. Phosphoproteomics has therefore been demonstrated to be an important tool for the comprehensive investigation and interpretation of cellular signaling events in proteomic studies.

Supplementary information

Table 4 Regulated peptides in the phosphoproteome. Green colored phosphosites are annotated with a biological function, blue phosphosites are annotated without biological function and red colored phosposites are not annotated in PhosphoSitePlus [17].

UniProt ID	UniProt Entry Name	Peptide	Log2 Fold Change	Adjusted P-value
O14523	C2C2L_HUMAN	R.SDISERPSVDDIE**pS[619]**E**pT[621]**GSTGALETR.S [605, 629]	-15.2554	0
O14523	C2C2L_HUMAN	R.SDISERPSVDDIE**pS[619]**ETG**pS[623]**TGALETR.S [605, 629]	-15.2644	0
Q15648	MED1_HUMAN	R.SQ**pT[1051]**PPGVA**pT[1057]**PPIPK.I [1048, 1061]	-14.5063	0
Q8TEV9	SMCR8_HUMAN	R.IPSAYPAGL**pS[698]pS[699]**DRHK.K [688, 702]	12.1688	0
P11171	41_HUMAN	R.QA**pS[521]**ALIDRPAPHFER.T [518, 532]	13.9144	0
P04439	HLAA_HUMAN	K.GG**pS[343]**YTQAASSDSAQGSDVSLTA**C**K.V [340, 363]	14.5272	0
O75396	SC22B_HUMAN	R.RNLG**pS[137]**INTELQDVQR.I [132, 146]	15.0722	0
Q14699	RFTN1_HUMAN	K.RPGNI**pY[20]pS[21]**TLKRPQVETK.I [14, 30]	15.7349	0
Q14699	RFTN1_HUMAN	K.RPGNIY**pS[21]pT[22]**LKRPQVETK.I [14, 30]	15.7359	0
P01100	FOS_HUMAN	R.KG**pS[362]**SSNEPSSD**pS[371]**LS**pS[374]**PTLLAL.- [359, 379]	17.069	0
P01100	FOS_HUMAN	R.KG**pS[362]**SSNEPSSD**pS[371]**L**pS[373]**SPTLLAL.- [359, 379]	17.0213	0
P01100	FOS_HUMAN	R.KG**pS[362]**SSNEPS**pS[369]**DSLS**pS[374]**PTLLAL.- [359, 379]	17.0039	0
P01100	FOS_HUMAN	R.KGS**pS[363]**SNEP**pS[368]**SDSLS**pS[374]**PTLLAL.- [359, 379]	17.0938	0
Q6F5E8	CARL2_HUMAN	K.AG**pS[1246]**DGDI**M**DSSTEAPPISIK.S [1243, 1262]	-15.4856	0.0001
Q5R372	RBG1L_HUMAN	R.ESDKEEPVTP**pT[473]**SGGGP**M**SPQDDEAEEESDNELSSGTGDVSKD**C**PEK.I [462, 507]	-15.6185	0.0001
Q92974	ARHG2_HUMAN	R.ERPSSAIYP**pS[127]**D**pS[129]**FRQSLLGSRR.G [117, 138]	13.2651	0.0001
P04439	HLAA_HUMAN	K.GG**pS[343]**YTQAASSDSAQGSDVSLTA**C**KV.- [340, 364]	13.4652	0.0001
Q15036	SNX17_HUMAN	R.R**pS[407]**DSQQAVK**pS[415]**PPLLESPDATR.E [405, 425]	13.5687	0.0001
Q09161	NCBP1_HUMAN	R.RK**pT[21]**SDANETEDHLESLI**C**K.V [18, 36]	14.4844	0.0001
P09693	CD3G_HUMAN	R.A**pS[148]**DKQTLLPNDQLYQPLK.D [146, 163]	15.0189	0.0001
Q9BZL6	KPCD2_HUMAN	R.LG**pT[211]**SESLP**C**TAEELSR.S [208, 223]	15.641	0.0001
Q05655	KPCD_HUMAN	R.A**pS[299]**RRSDSA**pS[306]**SEPVGI**pY[313]**QGFEK.K [297, 317]	16.6043	0.0001

Q05655	KPCD_HUMAN	R.ApS[299]RRpS[302]DSASSEPVGIYQGFEK.K [297, 317]	16.0512	0.0001
P01100	FOS_HUMAN	R.KGpS[362]SSNEPpS[368]SDSLSpS[374]PTLLAL.- [359, 379]	16.952	0.0001
P01889	HLAB_HUMAN	K.GGpS[343]YSQAACpS[350]DSAQGSDVSLTA.- [340, 361]	16.9591	0.0001
P29966	MARCS_HUMAN	K.GEPAAAAAPEAGApS[101]PVEKEAPAEGEAAEPGpS[118]PTAAEGEAASAASSTSSPK.A [87, 136]	17.1975	0.0001
O43561	LAT_HUMAN	R.EYVNVpS[224]QELHPGAAK.T [218, 232]	-14.0681	0.0002
P42345	MTOR_HUMAN	R.HASGANITNATTAATTAATATTTApS[1843]TEGSNSESEAESpT[1856]ENSPTPSPLQK.K [1818, 1866]	-16.0233	0.0002
Q86YP4	P66A_HUMAN	R.GVLHTFpS[546]PpS[548]PK.L [539, 549]	-14.4802	0.0002
Q9BRD0	BUD13_HUMAN	R.ARHDpS[271]PDLAPNVpT[279]YSLPR.T [266, 283]	-13.7017	0.0002
Q86UX7	URP2_HUMAN	R.TGSGGPGNHPHGPDApS[497]AEGLNPYGLVAPR.F [481, 509]	13.6649	0.0002
O94806	KPCD3_HUMAN	K.pT[389]ISPpS[393]TSNNIPLMR.V [388, 401]	14.673	0.0002
Q05655	KPCD_HUMAN	R.ApS[299]RRSDpS[304]ASSEPVGIpY[313]QGFEK.K [297, 317]	16.2386	0.0002
Q05655	KPCD_HUMAN	R.ApS[299]RRpS[302]DSASSEPVGIpY[313]QGFEK.K [297, 317]	16.2094	0.0002
Q9NQX3	GEPH_HUMAN	K.VKEVHDELEDLPSPPPPLpS[194]PPPpT[199]TSPHKQTEDK.G [175, 207]	-15.5189	0.0003
Q9BQY9	DBND2_HUMAN	R.TSSSSSSDSpS[222]pT[223]NLHSPNPSDDGADTPLAQSDEEEERGDGGAEPGACS.- [212, 258]	-14.1084	0.0003
Q9BQY9	DBND2_HUMAN	R.TSSSSSSDSSTNLHSPNPpS[231]DDGADpT[237]PLAQSDEEEERGDGGAEPGACS.- [212, 258]	-14.0842	0.0003
O94804	STK10_HUMAN	K.ApS[448]QpS[450]RPNSSALETLGGEK.L [446, 463]	-13.991	0.0003
P16949	STMN1_HUMAN	R.ASGQAFELILpS[25]PR.S [14, 26]	3.2289	0.0004
P01100	FOS_HUMAN	K.GSSSNEPSSDpS[371]LSpS[374]PTLLAL.- [360, 379]	13.6016	0.0004
P01100	FOS_HUMAN	K.GpS[362]SSNEPSSDSLpS[373]SPTLLAL.- [360, 379]	13.6017	0.0004
P01100	FOS_HUMAN	K.GpS[362]SSNEPSSDSLSpS[374]PTLLAL.- [360, 379]	13.5963	0.0004
Q05655	KPCD_HUMAN	R.RpS[302]DpS[304]ASSEPVGIYQGFEK.K [300, 317]	12.0541	0.0005
Q9ULC3	RAB23_HUMAN	K.IGVFNpT[196]pS[197]GGSHSGQNSGTLNGGDVINLRPNK.Q [190, 220]	13.2761	0.0006
Q5R372	RBG1L_HUMAN	R.ESDKEEPVTPpT[473]SGGGPMSPQDDEAEEESDNELSSGTGDVSK.D [462, 502]	-13.5932	0.0007
Q5R372	RBG1L_HUMAN	R.ESDKEEPVTPTSGGGPMSPQDDEAEEEpS[490]DNELSSGTGDVSK.D [462, 502]	-13.5791	0.0007

Q9UHD8	SEPT9_HUMAN	R.pS[30]FEVEEVEpT[38]PNSTPPRR.V [29, 45]	-13.3578	0.001
P01100	FOS_HUMAN	R.KGpS[362]SSNEPSSDpS[371]LSSPTLLAL.- [359, 379]	14.3523	0.0015
Q5W0Z9	ZDH20_HUMAN	R.pS[315]SGSNQPFPIKPLpS[328]ESK.N [314, 330]	12.7907	0.0016
P42566	EPS15_HUMAN	K.RpS[790]INKLDpS[796]PDPFK.L [788, 800]	12.888	0.0043
Q86YV0	RASL3_HUMAN	R.DGPPSALGpS[228]REpS[231]LApT[234]LSELDLGAER.D [219, 243]	-16.1282	0.0055
P42167	LAP2B_HUMAN	K.GGPLQALTREpS[250]pT[251]RGSR.R [239, 254]	5.9482	0.0063
P42167	LAP2B_HUMAN	K.GGPLQALpT[247]RESTRGpS[254]R.R [239, 254]	5.9467	0.0063
P01100	FOS_HUMAN	R.KGSSSNEPSSDSLpS[373]pS[374]PTLLAL.- [359, 379]	15.2323	0.0063
O75396	SC22B_HUMAN	R.NLGpS[137]INTELQDVQR.I [133, 146]	4.8793	0.0078
Q96TA1	NIBA2_HUMAN	K.AAPEASpS[692]PPApS[696]PLQHLLPGK.A [685, 704]	2.0041	0.0095
Q9Y6G9	DC1L1_HUMAN	R.KPVTVpS[510]PpT[512]TPTpS[516]PTEGEAS.- [504, 522]	5.833	0.0095
P04439	HLAA_HUMAN	R.KGGpS[343]YTQAASSDSAQGSDVSLTA**C**KV.- [339, 364]	4.7493	0.011
Q9BUA3	SPNDC_HUMAN	K.NLDPDPEPPSPDpS[251]PTETFAAPAEVR.H [238, 262]	-2.0807	0.0118
Q9BUA3	SPNDC_HUMAN	K.NLDPDPEPPpS[248]PDSPTETFAAPAEVR.H [238, 262]	-1.9621	0.0132
Q9BXB4	OSB11_HUMAN	R.SFSLASSSNpS[181]PISQR.R [171, 185]	-2.86	0.0148
Q3B726	RPA43_HUMAN	R.KHpS[316]EEAEFTPPLK**C**pS[328]PK.R [313, 329]	2.2357	0.0153
P11166	GTR1_HUMAN	R.QGGApS[473]QSDKTPEELFHPLGADSQV.- [468, 491]	5.1736	0.0171
P27361	MK03_HUMAN	R.IADPEHDHTGFLpT[202]EpY[204]VATR.W [189, 207]	3.7108	0.018
P17275	JUNB_HUMAN	R.DApT[255]PPVpS[259]PIN**M**EDQER.I [252, 267]	4.1444	0.0189
Q15742	NAB2_HUMAN	R.SFpS[159]PKpS[162]PLELGEK.L [156, 168]	4.2236	0.0194
Q15742	NAB2_HUMAN	R.pS[157]FSPKpS[162]PLELGEK.L [156, 168]	4.2312	0.0204
Q9UBC2	EP15R_HUMAN	R.pS[238]TPSHGSVSSLNSpT[251]GSLSPK.H [237, 256]	2.3713	0.022
Q6JBY9	CPZIP_HUMAN	R.RSpS[268]EEVDGQHPAQEEVPEpS[284]PQTSGPEAENR.C [265, 294]	4.3219	0.0222
Q6JBY9	CPZIP_HUMAN	R.RpS[267]SEEVDGQHPAQEEVPEpS[284]PQTSGPEAENR.C [265, 294]	4.0729	0.0222
Q09161	NCBP1_HUMAN	R.KpT[21]SDANETEDHLESLI**C**K.V [19, 36]	3.198	0.0244
O00567	NOP56_HUMAN	R.KFpS[563]KEEPVpS[569]pS[570]GPEEAVGK.S [560, 577]	3.1549	0.0271
P09693	CD3G_HUMAN	R.ApS[148]DKQTLLPNDQLYQPLKDR.E [146, 165]	5.4714	0.0271

P52594	AGFG1_HUMAN	K.SLLGDpS[167]APTLHLNKGTPpS[179]QSPVVGR.S [161, 185]	-3.6888	0.0284
P52594	AGFG1_HUMAN	K.SLLGDSAPpT[170]LHLNKGTPpS[179]QSPVVGR.S [161, 185]	-3.2457	0.0292
P52594	AGFG1_HUMAN	K.SLLGDSAPpT[170]LHLNKGTPSQpS[181]PVVGR.S [161, 185]	-3.129	0.0308
P52594	AGFG1_HUMAN	K.SLLGDpS[167]APpT[170]LHLNKGTPSQSPVVGR.S [161, 185]	-3.0709	0.0341
P52594	AGFG1_HUMAN	K.SLLGDSAPTLHLNKGpT[177]PSQpS[179]PVVGR.S [161, 185]	-3.0933	0.0355
Q9BXS6	NUSAP_HUMAN	K.LTTEATQpT[349]PVpS[352]NKKPVFDLK.A [341, 360]	-3.2345	0.0367
P16150	LEUK_HUMAN	K.GSGFPDGEGpS[336]SRRPpT[341]LTTFFGR.R [326, 347]	2.4994	0.0394
P52594	AGFG1_HUMAN	K.SLLGDSAPTLHLNKGpT[177]PpS[179]QSPVVGR.S [161, 185]	-3.1234	0.0401
Q6JBY9	CPZIP_HUMAN	K.A**M**VSPFHpS[120]PPSTPSSPGVR.S [112, 130]	-3.0592	0.0414
P49006	MRP_HUMAN	K.EGGGDSSASpS[120]PTEEEQEQGEIGA**C**SDEGTAQEGK.A [110, 143]	2.2754	0.0419
O00567	NOP56_HUMAN	K.FpS[563]KEEPVpS[569]pS[570]GPEEAVGK.S [561, 577]	4.2074	0.0419
P04439	HLAA_HUMAN	R.KGGSYTQAApS[349]SDSAQGSDVSLTA**C**KV.- [339, 364]	-1.9599	0.0442
O75995	SASH3_HUMAN	K.ALSEE**M**ADTLEEGpS[108]ASPpT[112]SPDYSLDSPGPEK.M [94, 124]	4.6229	0.0482
P98171	RHG04_HUMAN	R.QGLGPApS[896]TTSPSPGPRpS[906]PK.A [889, 907]	-2.7634	0.0485
P04439	HLAA_HUMAN	R.KGGSYTQAASSDSAQGpS[356]DVSLTA**C**KV.- [339, 364]	-2.4844	0.0498
Q9NQS7	INCE_HUMAN	K.ALNVTVDVQpS[798]PA**C**pT[802]SYQ**M**TPQGHR.A [788, 811]	-2.0591	0.0498
Q3B726	RPA43_HUMAN	R.KHSEEAEFpT[322]PPLK**C**pS[328]PK.R [313, 329]	2.1419	0.0498
Q9BSJ8	ESYT1_HUMAN	R.GpS[626]SVDAPPRP**C**HTTPDSQFGTEHVLR.I [624, 649]	4.5114	0.0498
O75995	SASH3_HUMAN	K.ALSEE**M**ADTLEEGSASPpT[112]pS[113]PDYSLDSPGPEK.M [94, 124]	4.8439	0.0498
Q86YV0	RASL3_HUMAN	R.VGpS[164]ApS[166]SEGSIHVA**M**GNFRDPDR.M [161, 182]	-2.6226	0.05

References

[1] https://smart.servier.com/, Creative Commons Attribution 3.0 Unported License.

[2] Matthiesen, R. (Ed.), *Mass spectrometry data analysis in proteomics*, Humana Press, New York, NY 2020.

[3] Ridgeway, M. E., Lubeck, M., Jordens, J., Mann, M., Park, M. A., Trapped ion mobility spectrometry: A short review. *International Journal of Mass Spectrometry* 2018, *425*, 22–35. doi:10.1016/j.ijms.2018.01.006.

[4] Bush, M. F., Hall, Z., Giles, K., Hoyes, J. et al., Collision cross sections of proteins and their complexes: a calibration framework and database for gas-phase structural biology. *Analytical chemistry* 2010, *82*, 9557–9565. doi:10.1021/ac1022953.

[5] Giles, K., Pringle, S. D., Worthington, K. R., Little, D. et al., Applications of a travelling wave-based radio-frequency-only stacked ring ion guide. *Rapid communications in mass spectrometry : RCM* 2004, *18*, 2401–2414. doi:10.1002/rcm.1641.

[6] Fernandez-Lima, F. A., Kaplan, D. A., Park, M. A., Note: Integration of trapped ion mobility spectrometry with mass spectrometry. *The Review of scientific instruments* 2011, *82*, 126106. doi:10.1063/1.3665933.

[7] Meier, F., Brunner, A.-D., Koch, S., Koch, H. et al., *Online parallel accumulation – serial fragmentation (PASEF) with a novel trapped ion mobility mass spectrometer* 2018.

[8] Meier, F., Beck, S., Grassl, N., Lubeck, M. et al., Parallel Accumulation-Serial Fragmentation (PASEF): Multiplying Sequencing Speed and Sensitivity by Synchronized Scans in a Trapped Ion Mobility Device. *Journal of proteome research* 2015, *14*, 5378–5387. doi:10.1021/acs.jproteome.5b00932.

[9] Wasinger, V. C., Cordwell, S. J., Cerpa-Poljak, A., Yan, J. X. et al., Progress with gene-product mapping of the Mollicutes: Mycoplasma genitalium. *Electrophoresis* 1995, *16*, 1090–1094. doi:10.1002/elps.11501601185.

[10] Martins-de-Souza, D., *Shotgun Proteomics*, Springer New York, New York, NY 2014.

[11] Pappin, D.J.C., Hojrup, P., Bleasby, A. J., Rapid identification of proteins by peptide-mass fingerprinting. *Current Biology* 1993, *3*, 327–332. doi:10.1016/0960-9822(93)90195-T.

[12] Henzel, W. J., Billeci, T. M., Stults, J. T., Wong, S. C. et al., Identifying proteins from two-dimensional gels by molecular mass searching of peptide fragments in protein sequence databases. *Proceedings of the National Academy of Sciences of the United States of America* 1993, *90*, 5011–5015. doi:10.1073/pnas.90.11.5011.

[13] Mann, M., Højrup, P., Roepstorff, P., Use of mass spectrometric molecular weight information to identify proteins in sequence databases. *Biological mass spectrometry* 1993, *22*, 338–345. doi:10.1002/bms.1200220605.

[14] The UniProt Consortium, UniProt: a worldwide hub of protein knowledge. *Nucleic acids research* 2019, *47*, D506-D515. doi:10.1093/nar/gky1049.

[15] Aebersold, R., Mann, M., Mass spectrometry-based proteomics. *Nature* 2003, *422*, 198–207. doi:10.1038/nature01511.

[16] Needham, E. J., Parker, B. L., Burykin, T., James, D. E., Humphrey, S. J., Illuminating the dark phosphoproteome. *Science signaling* 2019, *12*. doi:10.1126/scisignal.aau8645.

[17] Hornbeck, P.V, Zhang, B., Murray, B., Kornhauser, J.M., Latham, V., Skrzypek, E., PhosphoSitePlus, 2014: mutations, PTMs and recalibrations. *Nucleic Acids Res.* 2015, D512-520.

[18] Solari, F. A., Dell'Aica, M., Sickmann, A., Zahedi, R. P., Why phosphoproteomics is still a challenge. *Molecular bioSystems* 2015, *11*, 1487–1493. doi:10.1039/c5mb00024f.

[19] Humphrey, S. J., Karayel, O., James, D. E., Mann, M., High-throughput and high-sensitivity phosphoproteomics with the EasyPhos platform. *Nature protocols* 2018, *13*, 1897–1916. doi:10.1038/s41596-018-0014-9.

[20] Thingholm, T. E., Larsen, M. R., Ingrell, C. R., Kassem, M., Jensen, O. N., TiO(2)-based phosphoproteomic analysis of the plasma membrane and the effects of phosphatase inhibitor treatment. *Journal of proteome research* 2008, *7*, 3304–3313. doi:10.1021/pr800099y.

[21] Pan, C., Gnad, F., Olsen, J. V., Mann, M., Quantitative phosphoproteome analysis of a mouse liver cell line reveals specificity of phosphatase inhibitors. *Proteomics* 2008, *8*, 4534–4546. doi:10.1002/pmic.200800105.

[22] Wirbel, J., Cutillas, P., Saez-Rodriguez, J., Phosphoproteomics-Based Profiling of Kinase Activities in Cancer Cells. *Methods in molecular biology (Clifton, N.J.)* 2018, *1711*, 103–132. doi:10.1007/978-1-4939-7493-1_6.

[23] Giansanti, P., Aye, T. T., van den Toorn, H., Peng, M. et al., An Augmented Multiple-Protease-Based Human Phosphopeptide Atlas. *Cell reports* 2015, *11*, 1834–1843. doi:10.1016/j.celrep.2015.05.029.

[24] Dickhut, C., Feldmann, I., Lambert, J., Zahedi, R. P., Impact of digestion conditions on phosphoproteomics. *Journal of proteome research* 2014, *13*, 2761–2770. doi:10.1021/pr401181y.

[25] Fíla, J., Honys, D., Enrichment techniques employed in phosphoproteomics. *Amino acids* 2012, *43*, 1025–1047. doi:10.1007/s00726-011-1111-z.

[26] Li, X.-S., Yuan, B.-F., Feng, Y.-Q., Recent advances in phosphopeptide enrichment: Strategies and techniques. *TrAC Trends in Analytical Chemistry* 2016, *78*, 70–83. doi:10.1016/j.trac.2015.11.001.

[27] Liu, S., Zhang, C., Campbell, J. L., Zhang, H. et al., Formation of phosphopeptide-metal ion complexes in liquid chromatography/electrospray mass spectrometry and their influence on phosphopeptide detection. *Rapid communications in mass spectrometry : RCM* 2005, *19*, 2747–2756. doi:10.1002/rcm.2105.

[28] Boersema, P. J., Mohammed, S., Heck, A. J. R., Phosphopeptide fragmentation and analysis by mass spectrometry. *Journal of mass spectrometry : JMS* 2009, *44*, 861–878. doi:10.1002/jms.1599.

[29] Beausoleil, S. A., Villén, J., Gerber, S. A., Rush, J., Gygi, S. P., A probability-based approach for high-throughput protein phosphorylation analysis and site localization. *Nature biotechnology* 2006, *24*, 1285–1292. doi:10.1038/nbt1240.

[30] Savitski, M. M., Lemeer, S., Boesche, M., Lang, M. et al., Confident phosphorylation site localization using the Mascot Delta Score. *Molecular & cellular proteomics : MCP* 2011, *10*, M110.003830. doi:10.1074/mcp.M110.003830.

[31] Arrington, J. V., Hsu, C.-C., Elder, S. G., Andy Tao, W., Recent advances in phosphoproteomics and application to neurological diseases. *The Analyst* 2017, *142*, 4373–4387. doi:10.1039/c7an00985b.

[32] Posewitz, M. C., Tempst, P., Immobilized gallium(III) affinity chromatography of phosphopeptides. *Analytical chemistry* 1999, *71*, 2883–2892. doi:10.1021/ac981409y.

[33] Zhou, H., Ye, M., Dong, J., Corradini, E. et al., Robust phosphoproteome enrichment using monodisperse microsphere-based immobilized titanium (IV) ion affinity chromatography. *Nature protocols* 2013, *8*, 461–480. doi:10.1038/nprot.2013.010.

[34] Feng, S., Ye, M., Zhou, H., Jiang, X. et al., Immobilized zirconium ion affinity chromatography for specific enrichment of phosphopeptides in phosphoproteome analysis. *Molecular & cellular proteomics : MCP* 2007, *6*, 1656–1665. doi:10.1074/mcp.T600071-MCP200.

[35] Leitner, A., Phosphopeptide enrichment using metal oxide affinity chromatography. *TrAC Trends in Analytical Chemistry* 2010, *29*, 177–185. doi:10.1016/j.trac.2009.08.007.

[36] Yan, J., Li, X., Cheng, S., Ke, Y., Liang, X., Facile synthesis of titania-zirconia monodisperse microspheres and application for phosphopeptides enrichment. *Chemical communications (Cambridge, England)* 2009, 2929–2931. doi:10.1039/b901424a.

[37] Stechow, L. von (Ed.), *Phospho-Proteomics: Methods and Protocols*, Springer, New York, NY 2016.

[38] Yu, F., Qiu, F., Meza, J., in:, *Proteomic Profiling and Analytical Chemistry: The Crossroads*, North-Holland, [Erscheinungsort nicht ermittelbar] 2016, pp. 211–237.

[39] Karp, N. A., Huber, W., Sadowski, P. G., Charles, P. D. et al., Addressing Accuracy and Precision Issues in iTRAQ Quantitation*. *Molecular & cellular proteomics : MCP* 2010, *9*, 1885–1897. doi:10.1074/mcp.M900628-MCP200.

[40] Hogrebe, A., Stechow, L. von, Bekker-Jensen, D. B., Weinert, B. T. et al., Benchmarking common quantification strategies for large-scale phosphoproteomics. *Nature communications* 2018, *9*, 1045. doi:10.1038/s41467-018-03309-6.

[41] Beckerman, M., *Molecular and Cellular Signaling*, Springer Science+Business Media Inc, New York, NY 2005.

[42] Hunter, T., Sefton, B. M., Transforming gene product of Rous sarcoma virus phosphorylates tyrosine. *Proceedings of the National Academy of Sciences of the United States of America* 1980, *77*, 1311–1315. doi:10.1073/pnas.77.3.1311.

[43] Krishna, R. G., Wold, F., Post-translational modification of proteins. *Advances in enzymology and related areas of molecular biology* 1993, *67*, 265–298. doi:10.1002/9780470123133.ch3.

[44] Hunter, T., Protein kinases and phosphatases: The Yin and Yang of protein phosphorylation and signaling. *Cell* 1995, *80*, 225–236. doi:10.1016/0092-8674(95)90405-0.

[45] Bhullar, K. S., Lagarón, N. O., McGowan, E. M., Parmar, I. et al., Kinase-targeted cancer therapies: progress, challenges and future directions. *Molecular cancer* 2018, *17*, 48. doi:10.1186/s12943-018-0804-2.

[46] Yoshida, T., Zhang, G., Smith, M. A., Lopez, A. S. et al., Tyrosine phosphoproteomics identifies both codrivers and cotargeting strategies for T790M-related EGFR-TKI resistance in non-small cell lung cancer. *Clinical cancer research : an official journal of the American Association for Cancer Research* 2014, *20*, 4059–4074. doi:10.1158/1078-0432.CCR-13-1559.

[47] Mueller, B. K., Mack, H., Teusch, N., Rho kinase, a promising drug target for neurological disorders. *Nature reviews. Drug discovery* 2005, *4*, 387–398. doi:10.1038/nrd1719.

[48] Tabit, C. E., Shenouda, S. M., Holbrook, M., Fetterman, J. L. et al., Protein kinase C-β contributes to impaired endothelial insulin signaling in humans with diabetes mellitus. *Circulation* 2013, *127*, 86–95. doi:10.1161/CIRCULATIONAHA.112.127514.

[49] Sacco, F., Seelig, A., Humphrey, S. J., Krahmer, N. et al., *In vivo phosphoproteomics reveals pathogenic signaling changes in diabetic islets* 2018.

[50] Kato, A., Oda, S., Watanabe, M., Oyama, M. et al., Roles of the Phosphorylation of Herpes Simplex Virus 1 UL51 at a Specific Site in Viral Replication and Pathogenicity. *Journal of virology* 2018, *92*. doi:10.1128/JVI.01035-18.

[51] Rich, R. R. (Ed.), *Clinical immunology: Principles and practice*, Elsevier, St. Louis, Mo. 2019.

[52] Bosselut, R., S. Vacchio, M. (Eds.), *T-Cell Development: Methods and Protocols*, Humana Press, New York, NY 2016.

[53] Abraham, R. T., Weiss, A., Jurkat T cells and development of the T-cell receptor signalling paradigm. *Nature reviews. Immunology* 2004, *4*, 301–308. doi:10.1038/nri1330.

[54] Schneider, U., Schwenk, H. U., Bornkamm, G., Characterization of EBV-genome negative "null" and "T" cell lines derived from children with acute lymphoblastic leukemia and leukemic transformed non-Hodgkin lymphoma. *International journal of cancer* 1977, *19*, 621–626. doi:10.1002/ijc.2910190505.

[55] Durgan, J., Michael, N., Totty, N., Parker, P. J., Novel phosphorylation site markers of protein kinase C delta activation. *FEBS letters* 2007, *581*, 3377–3381. doi:10.1016/j.febslet.2007.06.035.

[56] Hellweg, C. E., Arenz, A., Bogner, S., Schmitz, C., Baumstark-Khan, C., Activation of nuclear factor kappa B by different agents: influence of culture conditions in a cell-based assay. *Annals of the New York Academy of Sciences* 2006, *1091*, 191–204. doi:10.1196/annals.1378.066.

[57] Tran, N. H., Zhang, X., Xin, L., Shan, B., Li, M., De novo peptide sequencing by deep learning. *Proceedings of the National Academy of Sciences of the United States of America* 2017, *114*, 8247–8252. doi:10.1073/pnas.1705691114.

[58] Kong, A. T., Leprevost, F. V., Avtonomov, D. M., Mellacheruvu, D., Nesvizhskii, A. I., MSFragger: ultrafast and comprehensive peptide identification in mass spectrometry-based proteomics. *Nature methods* 2017, *14*, 513–520. doi:10.1038/nmeth.4256.

[59] MacLean, B., Tomazela, D. M., Shulman, N., Chambers, M. et al., Skyline: an open source document editor for creating and analyzing targeted proteomics experiments. *Bioinformatics (Oxford, England)* 2010, *26*, 966–968. doi:10.1093/bioinformatics/btq054.

[60] Szklarczyk, D., Gable, A. L., Lyon, D., Junge, A. et al., STRING v11: protein-protein association networks with increased coverage, supporting functional discovery in genome-wide experimental datasets. *Nucleic acids research* 2019, *47*, D607-D613. doi:10.1093/nar/gky1131.

List of figures

List of tables

Acknowledgements

First of all, I would like to thank Univ.-Prof. Dr. Christopher Gerner for giving me the opportunity to perform my master's internship in his research group. I am very grateful for being able to perform research on a topic that truly interests me and for being given the possibility to get insights into and to be involved in so many different projects and topics. Subsequently, I would like to thank my co-supervisor and friend Lukas Janker for introducing me to the field of proteomics from the very beginnings during my bachelor's thesis, for teaching me basically everything I know about mass spectrometry and for enabling me to perform my master's thesis in the field of proteomics. Thanks to him, I was able to find true passion in my research that kept me going even through tough times of my thesis. Being one of my biggest emotional supporters during these times, I am truly thankful for his unconditional support both scientifically and personally. Furthermore, I would also like to thank Benjamin Neuditschko for patiently introducing me to cell culture techniques and friendly supporting me throughout my experiments. Moreover, I am very thankful for having Marlene Leibetseder as my companion during my thesis. She grew to be a very important friend of mine and I truly appreciated working together with her, especially during our cell culture experiments. A big thanks also goes to all the other members of the Gerner group for creating such a friendly atmosphere and for always having an open ear for any kind of concerns. I would also like to thank Giorgia del Favero from the department of food chemistry and toxicology for performing the fluorescence cell imaging. Big appreciation also goes to Martin Schaier for supporting me especially in the beginnings of my thesis and for always encouraging me to find my own way, independent from any circumstances. Last but not least, I am truly thankful for having my family as a support during my whole studies. Without their support, I would not have been able to perform any of my research and I would not be where I am today. I am especially thankful for the unconditional support I have always received from my mother, helping me to get where I am today.